Investigation of Near-Surface Mounted Method for Shear Rehabilitation of Reinforced Concrete T-Beams using CFRP Rods

Amir Mofidi[1], Omar Chaallal[2], Lijuan Cheng[3], and Yixin Shao[4]

ABSTRACT

This paper presents the results of an investigation of reinforced concrete (RC) T-beams retrofitted in shear with near-surface mounted (NSM) fibre-reinforced polymer (FRP) rods. Six full-scale 4520-mm-long RC T-beams were tested to study the effects of important parameters such as the presence of NSM FRP rods, the presence of steel stirrups, and the steel stirrup ratio. This paper provides an insightful and comprehensive description of the behaviour of strengthened T-beams under increasing load, from the formation of the first crack to ultimate failure. The results of this study and those gathered in the presented database show that existing steel stirrups and strengthening NSM FRP did not diminish each other's effect when failure modes unrelated to shear resistance of RC beams were prevented. The experimental results of this study and those in the database were used to verify a newly proposed model to predict the shear contribution of NSM FRP rods and laminates in RC beams strengthened in shear. The proposed model showed an improved accuracy compared to the existing models in the literature.

Keywords: Concrete beams; fibre-reinforced polymers; retrofitting; shear resistance; near-surface mounted; FRP rods; steel stirrups; design model.

[1] Postdoctoral Fellow, Department of Civil Engineering and Applied Mechanics, McGill University, 817 Sherbrooke West, Montreal QC Canada H3A 0C3; Department of Civil and Environmental Engineering, University of California, Davis (corresponding author). E-mail: amir.mofidi@mail.mcgill.ca.

[2] Professor of Construction Engineering, University of Quebec, École de Technologie Supérieure, 1100 Notre-Dame West, Montreal QC Canada H3C 1K3. E-mail: omar.chaallal@etsmtl.ca.

[3] Associate Professor, Department of Civil and Environmental Engineering, University of California, Davis, 3161 Ghausi Hall, One Shields Avenue, Davis, CA 95616. E-mail: dawcheng@ucdavis.edu.

[4] Associate Professor, Department of Civil Engineering and Applied Science, McGill University, Sherbrooke West, Quebec, Canada H3A 0C3. E-mail: yixin.shao@mcgill.ca.

INTRODUCTION

In recent years, fibre-reinforced polymer (FRP) composites as an innovative strengthening and rehabilitating material have been an attractive topic for practitioners and researchers (e.g., Seracino *et al.* 2007a; Kotynia 2007; Rizzo and De Lorenzis 2007; Galal and Mofidi 2009; Wiwatrojanagul *et al.* 2012; Pellegrino and Vasic 2013; and Mofidi *et al.* 2014). Near-surface mounted (NSM) FRP rods or laminates have provided a promising solution to the problem of shear strengthening (e.g., De Lorenzis and Nanni 2001; Barros and Dias 2006; Kotynia 2007). In this technique, FRP rods or laminates are embedded into pre-cut grooves on the concrete cover in the webs of RC beams. The idea was originated in 1940s when Asplund (1949) grouted NSM steel rods to strengthen a bridge slab in flexure. Fifty years later, Blaschko and Zilch (1999) and Nanni *et al.* (1999) proposed use of NSM FRP rods to rehabilitate RC beams in flexure.

Shear strengthening using NSM FRP method was investigated for the first time by De Lorenzis and Nanni (2001) through six RC beams, focusing on variables such as the spacing of the rods, the FRP rod inclination angle, the end-anchorage of the FRP rods, and the presence of internal steel shear reinforcement. In their study, a model was proposed to predict the contribution of NSM FRP rods for the shear resistance of RC beams. Later, the model was updated by Parretti and Nanni (2004) to be applicable to NSM FRP laminates in addition to NSM FRP rods. The model is still the most rational prediction tool proposed for RC beams strengthened with NSM FRP. However, it lacks a state-of-the-art bond model. The researchers assumed a constant value of 6.9 MPa as the average bond stress between FRP and concrete in their design equations. Although the proposed value was deemed practical at the early stages of the investigations on NSM method, further studies showed that the bond stress between NSM FRP and concrete is a function of several parameters including concrete strength and cross-sectional dimensions and shape of the NSM FRP material (e.g., De Lorenzis 2004 and Seracino *et al.* 2006b). Moreover, in their model the effective bond length of the FRP is limited by the cross-sectional dimensions of the RC beam or the corresponding length to FRP effective strain of 4000 με. However, further studies showed that the effective bond length of the NSM FRP is mainly a function of concrete strength, cross-sectional and mechanical characteristics of the FRP (e.g., Seracino *et al.* 2006).

Next group of research studies proposed a constant value for the effective strain of the FRP in their model. Barros and Dias (2006) conducted an investigation on eight rectangular RC beams strengthened with NSM FRP strips. The experimental parameters of their studies included the spacing of the strips, the FRP strips inclination angle, the presence of longitudinal steel reinforcement, and the presence steel stirrups. In their study, a bond stress of 16.1 MPa and an effective strain of 0.0059 were assumed to calculate the shear contribution of FRP. Kotynia (2007) performed eight tests on RC beams retrofitted in shear using NSM laminates. The test parameters included the inclination and spacing of the FRP laminates. The findings suggested that the effective strain in NSM FRP could be assumed as 0.0035 to predict the FRP shear contribution. Anwarul Islam (2009) conducted tests on three RC beams retrofitted in shear with NSM FRP rods to study the effects of NSM FRP rod spacing and the presence of steel stirrups. The results suggested that the NSM effective strain should be taken as one-third of the ultimate strain of the FRP rods in calculating the FRP shear contribution. It is now established that the effective strain of the FRP is dependent on several parameters including the mechanical properties, shape, inclination of the NSM FRP and concrete strength (e.g., Dias and Barros 2013). Taking the effective strain of the FRP in the abovementioned studies as a constant value might not lead to accurate predicted results.

Several experimental studies were conducted on different test variables without proposing separate design equations to predict the behavior of the strengthened specimens. In the investigation by Rizzo and De Lorenzis (2007), the effectiveness of FRP rods versus FRP strips was evaluated in addition to the effects of various adhesives, FRP reinforcement inclination angle, and spacing between FRP reinforcements. Wiwatrojanagul *et al.* (2012) studied the effect of FRP rod materials (Aramid FRP versus Carbon FRP), the inclination and the spacing of FRP rods on six shear strengthened RC beams with NSM FRP rods. They concluded that decreasing the spacing between FRP rods did not necessarily lead to increases in the shear capacity of the strengthened specimens, since this might lead to concrete cover splitting type of failure mode. Rahal and Rumaih (2011) investigated the effect of FRP rods inclination, FRP rods end-anchorage and NSM FRP rods type (FRP versus steel rods) on three 3250 mm-long RC beams. Extending the NSM rods into one specimen's concrete flange increased the shear resistance and prevented the concrete cover splitting in the specimen. Cisneros *et al.* (2012) studied the effect of the inclination, the cross-sectional shape (rods versus strips) and the spacing of the NSM FRP composites on sixteen test specimens. Raj and Surumi (2012) tested ten shear strengthened rectangular RC specimens using NSM FRP rods and strips. The test parameters were the FRP strips/rods inclinations and the spacing between the FRP rods/strips. Jalali *et al.* (2012) investigated the effectiveness of man-made NSM FRP rods in shear retrofit of five rectangular RC beams. The spacing of the FRP rods, the FRP rod angle, and the end-anchorage of the FRP rods were the experimented parameters of their study. Their proposed end-anchorage man-made FRP rods enhanced the shear resistance and the ductility of the test specimens. Note that most of RC beams in these studies had a span length shorter than 4 m (small-scale or medium-scale specimens). Currently, there is a lack of large-scale test specimen in the literature for full-scale

RC beams strengthened with NSM FRP. The size effect of RC beams strengthened with NSM FRP can be particularly important. This is due to the fact that the concrete cover thickness plays an utterly vital role in beams strengthened with NSM FRP method. The concrete cover thickness is not proportionately down-scaled compared to the rest of RC beams dimensions for a small- or medium-scale test specimen.

Dias and Barros (2008, 2010, 2011, and 2012) conducted comprehensive series of tests to strengthen RC beams with NSM FRP laminates. The test variables in their separate studies included concrete compressive strength, pre-cracking of the specimens, internal steel shear reinforcement, the spacing of the FRP reinforcement, and the FRP reinforcement angle. Based on their experimental results, they proposed a new design model for NSM FRP laminates (Dias and Barros 2013). According to their model, the presence of steel stirrups decreases the effective strain in NSM FRP laminates. The effective strain in the FRP is calculated based on curve fitting of the experimental results of their own test as a function of the sum of the rigidity of transverse steel reinforcement and that of transverse NSM FRP and concrete compressive strength. Although several studies have pointed out that the presence of steel stirrups has a diminishing effect on the shear contribution of FRP for RC beams strengthened with Externally-Bonded (EB) method (e.g., Mofidi and Chaallal 2011; Mofidi *et al.* 2012b; Pellegrino and Vasic 2013; Mofidi and Chaallal 2014a-b), such effect has not been thoroughly investigated for RC beams strengthened with NSM FRP method and its occurrence is in doubt.

This need is the main impetus of this study to conduct an extensive, comprehensive, and targeted experimental investigation involving six full-scale 4520-mm-long T-beams with different steel shear reinforcement ratios. The results of this study (and those available in literature) have been used to study the mechanism of shear resistance for RC beams strengthened with NSM FRP and investigate a possible interaction between steel and FRP shear reinforcement. Moreover, a reliable design method have been proposed for shear strengthening of RC beams with NSM FRP rods and laminates that uses a state-of-the-art bond model and can predict possible failure modes. The accuracy of the predicted results have been verified using collected experimental data from the published studies on shear strengthening of RC beams using NSM FRP composites and compared with the results predicted by aforementioned design models proposed by other researchers.

EXPERIMENTAL PROGRAM

Description of specimens

The experimental program involved six tests performed on full-scale, 4520-mm-long RC T-beams (Table 1). The T-section had overall dimensions of 508 mm (flange width) by 406 mm (total depth). The thicknesses of the web and flange were 152 and 102 mm respectively (Fig. 1). The control specimens not strengthened with carbon FRP (CFRP) rods were labelled as CON. The specimens labelled as NR were RC T-beams with no internal transverse-steel stirrups. The specimens labelled as MR (moderately reinforced with internal transverse-steel reinforcement) and HR (heavily reinforced with internal transverse-steel reinforcement) had steel stirrups spaced at $s = 3d/4$ for MR and $s = d/2$ for HR, where $d = 350$ mm was the effective depth of the beam cross-section. The specimens in this study are representative of RC elements designed prior to modern codes and therefore the beams in the HR series are qualified as heavily reinforced. In addition, the maximum steel stirrup spacing values proposed by modern codes, $0.5d$ in ACI 318-11 or $0.7d_v$ in A23.3-14 (where d_v is the greater of $0.9d$ or $0.72h$, h is the height of the member) are for design and field practice to avoid brittle shear failure. This limit, however, is conservative for shear strengthening research purposes. The specimens strengthened with NSM were labelled as NSM. The spacing between the NSM FRP rods was 130 mm for all the strengthened specimens.

The longitudinal steel reinforcement consisted of four 25M bars (diameter 25.2 mm, area 500 mm^2) laid in two layers at the bottom and six 10M bars (diameter 10.3 mm, area 100 mm^2) laid in one layer at the top. The bottom bars were anchored at the support with 90-degree hooks to prevent premature anchorage failure. The steel stirrups (where applicable) were 8 mm in diameter (area 50 mm^2). The longitudinal steel reinforcement had a nominal yield strength of 470 MPa for the NR and HR series and 650 MPa for the MR series. The steel stirrups had a nominal yield strength of 540 MPa for the HR series and 650 MPa for the MR series.

A commercially available concrete delivered to the laboratory by a local supplier was used. The specimens were cast in two phases using separate concrete batches of the same mix design and supplier. NR-CON, HR-CON, NR-NSM, and HR-NSM specimens were cast in the first phase and MR-CON and MR-NSM specimens in the second phase. Standard compression tests on control cylinders yielded an average 28-day concrete compressive strength of 25.0 MPa and 29.6 MPa for the first and second phases respectively. For each concrete batch, the scatter among the compression test results for the cylinder specimens was negligible.

To apply the NSM FRP shear strengthening system, the following steps were performed: (1) grooves of 15 mm width and 15 mm depth and spaced at 130 mm were made on both lateral sides of the beam; (2) the grooves were cleaned by compressed water and air; (3) two-third of the grooves' volume was filled with epoxy blended according to the supplier's recommendations; (4) a thin layer of the supplier's epoxy adhesive was applied around the 9.5-mm-diameter CFRP rods; (5) the 9.5-mm-diameter CFRP rods were installed into the groove on both sides of the beam; and (6) the excess epoxy adhesive was removed.

Sand-coated CFRP rods were used to strengthen the RC T-beams. The tensile strength, elongation at break, and modulus of elasticity of the sand-coated CFRP rods were 1885 MPa, 1.27% and 148 GPa respectively. The reported results are the mean values of several test results conducted on the steel bars, concrete specimens and CFRP rods. The mechanical properties of the adhesive as specified by the manufacturer were: 21 MPa bond strength, 1% elongation at break, 75 MPa compressive strength, and 3656 MPa compressive modulus.

Test setup and instrumentation

All T-beam specimens were tested in a simply supported three-point bending configuration, as shown in Fig. 1. The load was applied at a distance $a = 3d$ from the nearest support, which corresponds to the case of a slender beam in which the shear resistance is governed by the beam action mechanism. The vertical displacement of the beam was measured at the position under the applied load using linear variable differential transducers (LVDT, 150 mm measuring range). The longitudinal steel reinforcement was instrumented with a strain gauge at the point of loading. Strain gauges were also installed on the transverse-steel stirrups located in the loading zone along the anticipated plane of shear failure. The deformations experienced by the CFRP rods were measured using strain gauges installed on the rods. These gauges were attached vertically to the CFRP rods before the rods were epoxy-bonded into the pre-cut grooves. The maximum strain range of the strain gauges used in this study was 2% per manufacturer’s data.

EXPERIMENTAL RESULTS

Overall response

Table 2 summarizes the overall experimental results obtained from the tests for all specimens. The results are presented in terms of the loads attained at failure, the experimental shear resistance due to concrete, steel stirrups, and CFRP, and the percent shear capacity gain due to CFRP, defined as $(V_f)/(V_{total} - V_f)$, where V_{total} is the total load at failure. In deriving some of the values in Table 2, the following assumptions were made: (a) the shear resistance due to concrete was the same whether or not the beam was retrofitted in shear with FRP and whether or not the retrofitted beam was reinforced with transverse steel; and (b) the contribution of steel stirrups was the same for both strengthened and unstrengthened beams.

Crack Pattern and Failure Mode

The load level at which the first diagonal shear crack occurred was of similar magnitude for all specimens. During the loading of control specimen NR-CON (unstrengthened and with no steel stirrups), diagonal shear cracks initiated at the centre of the shear span at a load of 78.8 kN. As the load increased, only one crack widened and propagated until final failure, which occurred at a load level of 122.7 kN. An MR-CON beam (unstrengthened but with steel stirrups spaced at 260 mm) experienced the first diagonal shear crack at a load (79.2 kN) similar to that in NR-CON, but the final failure occurred at a much higher load (294.0 kN) due to rupture of a steel stirrup. An HR-CON beam (with steel stirrups spaced at 175 mm) showed similar behaviour, with the ultimate load reaching 350.6 kN, also due to rupture of a steel stirrup.

Among the NSM-strengthened specimens, beam NR-NSM (no steel stirrups, but retrofitted with 9.5-mm-diameter NSM vertical rods spaced at 130 mm) failed when the load reached 198.0

kN. This corresponds to a 61% increase in shear capacity with respect to the control beam, NR-CON. Only one diagonal shear crack formed in this beam at an angle of 47°, widening and propagating as the applied load increased. A popping noise was noted throughout the test, revealing the progressive cracking of the specimen. This caused splitting of the concrete cover in which two thick layers of concrete cover (including the NSM FRP rods) split off from the sides of the beam. After losing the NSM rods (no bond stress transfer between FRP and concrete), the beam finally failed in a diagonal tension failure mode.

For specimens with steel stirrups and strengthened with NSM (i.e., MR-NSM and HR-NSM), parallel diagonal cracks started to open up at relatively equal spacing and at an angle of 43° to 47° with respect to the beam axis. Figure 2 shows the spacing between these shear cracks in specimen MR-NSM at failure, where the ultimate load reached 380.0 kN, which is 29.2% greater than the capacity of the corresponding control beam MR-CON. The final failure was in shear due to concrete-cover splitting (Fig. 2). For beam HR-NSM, the ultimate load was 365.0 kN, which was 4% greater than the capacity of the corresponding control beam HR-CON before the global flexural failure mode occurred.

Deflection response

Figure 3 shows the curves representing load versus maximum deflection at the loading point for all specimens. The quasi-linear behaviour of curves corresponding to the control beams and NR-NSM specimens is characteristic of a typical shear failure. It can be seen that the NSM method generally enhanced the overall behaviour of the RC beams. Compared to the unstrengthened control specimens, the strengthened T-beams had higher ultimate loads at failure (61%, 29%, and 4% for NR-NSM, MR-NSM, and HR-NSM respectively) and greater maximum deflections (234%, 4%, and 10% for NR-NSM, MR-NSM, and HR-NSM respectively) compared to their corresponding control specimens. All the tested beams except HR-NSM exhibited a brittle type of behaviour, which was characterized by a sudden drop in the load-displacement curves after the peak load (Fig. 3). In contrast, beam HR-NSM showed a ductile behaviour and failed in flexure.

Strain response

To obtain a better understanding of the shear resistance mechanism in the strengthened beams, extensive instrumentation was installed for strain monitoring, especially in steel stirrups and NSM rods.

Transverse-steel reinforcement — Figure 4 presents the response of applied load versus maximum measured strain in the transverse-steel stirrups for the MR and HR series that contained steel stirrups. These behaviour curves indicate that the steel stirrups went through three phases during loading. In the initial phase (phase "A"), no noticeable contribution of the transverse steel to shear resistance was observed. In the second phase (phase "B"), the first diagonal cracks initiated, and the steel stirrups started to contribute to shear resistance. This phase started at an average applied load of approximately 75.0 kN for most specimens (Fig. 4). This is close to the failure load of the unreinforced control specimen (NR-CON) at 78.8 kN and the crack opening load of the control specimen with steel stirrups (MR-CON) at 79.2 kN. Therefore, the ending load of phase "A" (starting load of phase "B") is considered as the cracking load of the concrete specimens in this study. After Phase B (in the third phase), the strain in the steel stirrups continued to increase with increasing load at a greater rate than in the second phase until ultimate failure of the specimen. It was also found that the maximum strain in the steel stirrups that intercepted the principal shear crack became greater than the yielding strain (as labelled in Fig. 4) by a significant margin before the specimen failed.

Figure 4 also shows that, under the same applied load, the strain level in the steel stirrups was substantially greater in the unstrengthened control specimens with no CFRP. This implies that the presence of NSM CFRP eased the strain in the transverse-steel stirrups. Moreover, yielding of the steel stirrups occurred earlier in specimens with wider spacing between steel stirrups (MR series) than in beams with tighter spacing between steel stirrups (HR series), although in MR series the yield point of the stirrups was greater than that of HR series (i.e., 650 MPa versus 540 MPa).

NSM CFRP rods — Figure 5 shows the load versus maximum measured strain behaviour in the NSM CFRP rods in the strengthened specimens. The maximum strain was measured in the NSM rods that intercepted the major shear crack on both sides of the RC beams. Note that all the strain values reported in this paper are the maximum measured (captured) values. They are not necessarily the absolute maximum values experienced by the NSM rods (i.e., in cases where the strain gauges did not intercept the principal cracks). The curves in Fig. 5 display a similar tendency to those for steel stirrups, except for the last phase. The CFRP rods did not make much contribution during the initial stage (Phase "A") of loading, but began to stretch at an applied load of 100.0 kN on average for all three series. In the last stage, however, the CFRP strain started to decrease, drastically at times, as the load increased (e.g., HR-NSM-Right, where the curve shows a reversing portion, indicating a strain decrease in the FRP with increasing load). This strain decrease can be related to local concrete cover splitting which reduced the shear transfer between the NSM FRP and the RC beams' concrete core, accompanied by concrete cracking noises in the beams during loading.

Behaviour of Strengthened RC Beams under Increasing Load

The local behaviour of steel stirrups and NSM rods, particularly within the failure zones, is next discussed and analyzed in depth. To enhance the reliability of the results, the measured strain gauge data are further compared with associated crack formation and with patterns that are closely related to one another.

Analysis of Steel Stirrup Behaviour at Failure

Figure 6 shows the measured strain distribution at failure among the steel stirrups (S1-S4) for series MR and HR. The strain curves in solid black bars on the stirrups are drawn to scale. A horizontal line near the bottom of the beam indicates the yield point of the steel stirrups (MR: $\varepsilon_y = 0.0033$; HR: $\varepsilon_y = 0.0027$). The inclination of the plane of rupture is assumed to be equal to the principal crack angle with respect to the longitudinal axis as measured at the end of the test. Although the cracking pattern in some specimens was distributed throughout the shear span, the principal shear crack was taken as the crack that passed through the entire cross section of the beams and led to ultimate shear failure. In addition to the strain at ultimate failure in each stirrup, Fig. 6 also shows the applied forces corresponding to the yield point (F_{yield}) of each stirrup at the bottom of each beam (stacked bars). These loads are reported as a percentage of ultimate load ($F_{ultimate}$) reached. The number beside each yielded stirrup indicates its sequence of yielding. Based on Fig. 6, the following observations can be made:

1. In general, the stirrups crossing the principal shear crack were highly strained. Yielding of the steel stirrups was observed in all cases.

2. For the unstrengthened control specimens (MR-CON and HR-CON), the stirrup located in the critical section yielded first, followed by the other stirrups. This corroborates the observation that the first diagonal crack appeared in the beam web, midway between the support

and the load application point. As the load increased, these cracks became wider and progressed simultaneously toward both the support and the load point. For the strengthened specimens (MR-NSM and HR-NSM), the first steel stirrup to yield was not located in the plane of ultimate failure. Proper strengthening of the specimens resulted in formation of concrete struts throughout the shear span of the RC beams, leading to a distributed cracking pattern. In this case, the first shear crack that caused the first steel stirrup to yield was not necessarily the principal shear crack that led to ultimate shear failure, e.g., stirrup S4 yielded first in specimen MR-NSM, but the principal shear crack passed through stirrup S3. Similar behaviour was observed in specimen HR-NSM, where stirrup S3 yielded first, but the principal shear crack passed through stirrup S2.

3. For the unstrengthened control specimens, yielding of steel stirrups began under a load much less than ultimate load, starting at 69% and 81% of ultimate force for specimens MR-CON and HR-CON respectively. On the other hand, for NSM-strengthened beams, yielding of steel stirrups occurred under higher shear loads, between 94% and 100% of ultimate load. This means that the presence of NSM FRP rods delayed yielding of steel stirrups. However, after stirrup yielding, the residual capacity of the specimens became minimal, if not negligible.

4. For specimen MR-CON, the strain in the steel stirrups was not well distributed (only stirrups S2 and S3 that intercepted the principal shear crack were significantly strained). This could have been due to the wider spacing between steel stirrups (260 mm) in this specimen, which allowed the major shear crack to pass through the concrete cross section under a lower applied force than in the HR-CON specimen, which had a stirrup spacing of 175 mm. For the NSM-strengthened specimens (MR-NSM and HR-NSM), strengthening using NSM led to formation of concrete struts throughout the specimens' shear spans. This resulted in a much more

even strain distribution among the steel stirrups in the strengthened beams (e.g., MR-NSM) than in the unstrengthened ones (e.g., MR-CON).

Analysis of NSM FRP Rod Behaviour at Failure

The distribution of maximum strain attained by the NSM CFRP rods (F1-F5) on both sides of the RC beams is shown in Fig. 7 for the three NSM-strengthened specimens. The clustered bars on each side of the FRP rods (labelled as L and R) are drawn to scale. The applied forces corresponding to the maximum strain on the FRP ($F_{\varepsilon\text{-}max}$) are also indicated at the bottom of each beam's figure (stacked bars) in terms of a percentage of ultimate force reached (F_u). The following observations were made based on Fig. 7:

1. Similarly to the strain in steel stirrups, the NSM FRP rods crossing the principal shear crack were strained the most. The maximum strain in CFRP rods was generally greatest in the middle of the failure zone where the first diagonal cracks initiated and propagated simultaneously towards the support and the compression flange. This non-uniform strain distribution in the CFRP rods over the failure zone shows the importance of the CFRP anchorage length available, which was less for the NSM rods at both ends than for rods in the middle of the failure zone.

2. In specimen NR-NSM, although the strengthening NSM FRP proved very effective, the strain in the FRP rods was not well distributed with respect to the shear span. This could have been due to the absence of internal steel stirrups, which prevented proper formation of concrete struts across the shear span. Only NSM rods F3 and F4, which intercepted the principal shear crack, were significantly strained. The rest of the FRP rods did not efficiently contribute to shear resistance. This occurred because the specimen failed in a single-crack pattern which did not intercept FRP rods F1, F2, or F5. These NSM rods reached their maximum strain under a lower

load (i.e., they stopped contributing to shear resistance before ultimate failure) compared to the rest of the NSM rods. However, in specimens MR-NSM and HR-NSM, shear strengthening of specimens with NSM FRP resulted in a better strain distribution with respect to the shear span than that in the unreinforced specimen (NR-NSM). This could have been due to formation of concrete struts throughout the specimens' shear spans.

3. Some of the NSM rods in the critical zone that were significantly strained reached their maximum strain level under a load less than the maximum load at failure (e.g., F2 in MR-NSM and F3 in HR-NSM). This could have been due to local cracks in the concrete cover or to local debonding of NSM rods that stopped shear transfer between the NSM CFRP rods and the surrounding concrete prior to ultimate failure.

Effect of Steel Shear Reinforcement on the Contribution of NSM FRP to Shear Resistance

One of the test parameters of the current study is this effect of transverse-steel shear reinforcement on the FRP contribution of RC beams strengthened with NSM FRP for shear resistance. For specimens NR-NSM (no transverse reinforcement) and MR-NSM (moderate transverse reinforcement), Table 2 shows that the FRP shear contribution slightly increased instead of decreasing in the presence of steel stirrups (i.e., 56.9 kN for MR-NSM versus 49.8 kN for NR-NSM). In other words, the presence of steel stirrups did not diminish the NSM FRP's shear contribution. Unlike in the EB FRP method, the highly stressed areas around NSM FRP do not significantly overlap/interact the highly stressed areas around the existing steel stirrups. This is mainly due to the fact that the location of the NSM FRP rods is generally taken with distance away from the location of steel stirrups to avoid possible damage to the steel stirrups during groove cutting for NSM FRP. Therefore, the bond quality between the NSM FRP and the concrete is not compromised by the presence of the steel stirrup. Note that in the specimens with steel stirrups (MR-CON, HR-CON, MR-NSM, and HR-NSM), shear failure occurred after the steel stirrups intersecting the principal crack had yielded (i.e., the steel contribution to shear resistance was not affected by the presence of the strengthening FRP). Therefore, similar equations can be used to calculate the shear contribution of steel for both unstrengthened and strengthened specimens.

In order to better investigate this effect with more experimental results, a database of more than 69 RC beams strengthened with NSM FRP rods and laminate that failed due to NSM FRP strengthening system failure (debonding or concrete cover splitting) was collected (Table 3). The database includes most of the relevant data in the existing literature of the tested beams strengthened with NSM FRP including the geometric properties of the test specimens and of the FRP composites, the elastic and mechanical properties of the materials used, and the load at failure (V_{total}), and the contribution of the FRP to shear resistance (V_f).

Fig. 8 displays the FRP shear contribution for NSM-strengthened RC beams versus the internal steel stirrup reinforcement ratios, $\rho_{sv} = (A_{sv}) / (b_w \times s)$, where A_{sv} and s are the total area of the cross-section and the spacing of the transverse steel reinforcement. Fig. 8 clearly shows that the shear contribution of FRP did not decrease (in fact slightly increased when considering a linear trend line) with the increase in the shear transverse reinforcement ratio. Furthermore, in order to normalize the shear contribution of FRP for RC beams with different cross-sectional dimensions, the variations of the strengthening factor κ_f versus the increases in ρ_{sv} is represented in Fig. 9. The FRP strengthening factor κ_f is defined as $(V_f)/(V_{max})$, where $V_{max} = 0.25 f'_c\, b_w\, d_v$ is the maximum shear resistance of the cross-section based on CSA A23.3-14. Fig. 9 reveals that the FRP strengthening factor slightly increases when the steel shear reinforcement ratio increases. It can be concluded that unlike EB FRP method, the presence of the internal steel shear reinforcement does not influence the contribution of FRP to the shear resistance for shear-strengthened RC beams with NSM FRP method. These results are in correlation with the experimental results of this study and those reported by De Lorenzis and Nanni (2001) among others.

PROPOSED SHEAR DESIGN EQUATIONS

For practical design purposes, a design model is proposed in this paper for RC beams strengthened in shear using NSM FRP rods and laminates, which can predict possible failure modes including debonding of FRP and concrete-cover splitting.

Description of model

For RC beams strengthened with NSM FRP rods and laminates, the FRP contribution to shear resistance can be written in the following form (Kotynia 2007, Anwarul Islam 2009, Jalali *et al.* 2012):

$$V_f = \frac{A_f \cdot E_f \cdot \varepsilon_{fe} \cdot d_{fv}}{s_f} \tag{1}$$

where A_f, E_f, d_{fv}, ε_{ef}, and s_f are respectively the FRP cross-sectional area on both sides of the beam, the FRP rod or laminate modulus of elasticity, the effective shear depth of the cross-section, the effective strain in the FRP rod or laminate, and the spacing between the NSM FRP rods or laminates. The effective shear depth can be taken as the greater of $0.72h$ and $0.9d$ as per CSA/S806 (2012). The FRP effective strain is the average of the maximum strain experienced by the actively involved FRP rods or laminates at the ultimate point. Precise predictions of effective strain for all potential failure modes of the specimen constitute an important step towards achieving accuracy in calculating the FRP shear contribution at the ultimate loading stage. The corresponding FRP effective strain at the ultimate point due to the applicable failure mode should be evaluated on each side of the major shear crack. Because failure occurs on the side of the crack with the lesser effective strain corresponding to an applicable failure mode, the value of the lesser effective strain is the governing effective strain and should be used in Eq. (1) to calculate the FRP contribution to shear resistance.

Failure due to Debonding of NSM FRP at the Concrete/Epoxy Interface

Debonding of NSM FRP is a common failure mode for RC beams strengthened using NSM FRP (De Lorenzis and Nanni 2001; Rizzo and De Lorenzis 2007). According to previous experimental pull-off tests on NSM FRP plates, debonding at the concrete/epoxy interface has been the major failure mode among all the failure modes considered (Blaschko 2003; Seracino *et al.* 2007a). Failure at the concrete/epoxy interface is characterized by cracking in the concrete layer adjacent to the epoxy-bonded layer. The FRP ultimately debonds from the concrete surface with a thin layer of concrete (in some cases, only mortar with no aggregate attached to the FRP). According to Seracino *et al.* (2007b), the pull-off force (P_{fb}) of the CFRP laminate at the concrete/epoxy interface (failure by cracking in the concrete layer adjacent to the epoxy-bonded layer) can be calculated as follows:

$$P_{fb} = 0.85 \varphi_f^{\ 0.25} \cdot f_c'^{\ 0.33} \sqrt{L_{per} E_f A_f} \qquad (2)$$

where units of Newtons and millimetres are used, φ_f is the debonding-failure plane aspect ratio and is equal to $(d_f)/(b_f)$; b_f is the length of the failure plane parallel to the concrete surface (at the FRP/concrete interface), which for NSM laminates and rods is taken to be the width of the groove plus 2 mm; and d_f is the length of the failure plane perpendicular to the concrete surface, which for NSM plates is taken to be the depth of the groove plus 1 mm, where width and depth of the groove in the current study are taken equal to 1.5 times the rod diameter (based on pull-off tests of Wiwatrojanagul *et al.* 2012). The other important parameter in Eq. (2) is L_{per}, which is the debonding failure plane in cross section and was set equal to ($2d_f + b_f$) under the assumption that the effective bond length (L_{ef}) of the FRP plates or rods was fully available. However, for RC beams strengthened in shear with NSM FRP, the effective length of the FRP might not always be physically available. The effective bond length is the length beyond which any increase in bond length does not translate into an increase in bond force. The pull-off force of the NSM FRP at the concrete/epoxy interface is a linear function of the embedment length of NSM FRP rods on both sides of the major crack, where the effective bond length represents the upper bound of FRP bond length (Seracino *et al.* 2007a). According to Seracino *et al.* (2007b), the effective bond length of the NSM FRP plates is given by:

$$L_{ef} = \left(\frac{\pi}{2\lambda}\right) \tag{3}$$

$$\lambda^2 = \left(\frac{\tau_{max} L_{per}}{\delta_{max} E_f A_f}\right) \tag{4}$$

where

$$\tau_{\max} = (0.802 + 0.078\varphi_{\mathrm{f}})\, f_c'^{\,0.6} \tag{5}$$

$$\delta_{max} = \left(\frac{0.976\varphi_f^{\,0.526}}{0.802 + 0.078\varphi_f}\right) \tag{6}$$

where units of Newtons and millimetres are used, λ is a constant, and τ_{max} and δ_{max} are respectively the maximum shear stress and the maximum slip, assuming a bilinear bond-slip relationship at the concrete/epoxy interface. The maximum shear stress and maximum slip were calculated on the basis of an empirical equation extracted from a statistical analysis (Seracino *et al.* 2007a).

As mentioned earlier, in many shear-strengthening field cases, the effective length of the FRP might not always be physically available. For this case, a modification factor (k_{ef}) is proposed in this study to account for the effect of effective bond length in calculating the corresponding maximum FRP strain for the debonding failure mode, i.e.,

$$k_{ef} = \left(\frac{k_g L_{total}}{L_{ef}} \right) \tag{7}$$

where k_g is an experimental coefficient to consider the group effect (the original bond model was calibrated for single NSM FRP bonded to concrete blocks) for all active NSM FRP rods and laminates (k_g is taken equal to 0.75 and 0.50 for rods and laminates, respectively), L_{total} is the total length of the NSM FRP rods or laminates that are actively contributing to shear resistance (i.e., intersecting the principal shear crack with proper bond length on both sides of the crack) at ultimate failure. Therefore, L_{total} is the sum of the shorter parts of all NSM FRP rods or laminates that pass the 45 degrees major shear crack (as illustrated in Fig. 10 for a template cross-sectional size and NSM FRP spacing), where the upper bound of the shorter part of NSM FRP rods or laminates is L_{ef}. In Fig. 10, L_1 is the dimension of the shorter part of the first NSM FRP that passes the shear crack. L_2 and L_3 are the dimensions of the shorter parts of the second and the third NSM FRP that pass the shear crack, the dimensions of which are limited by the upper bound, i.e., L_{ef}. L_4 is the dimension of the shorter part of the last NSM FRP and is represented by term r_f in the general form calculations below. The total length, L_{total}, is indeed a parameter dependent on beam size (d_{fv}), NSM FRP spacing (s_f), and effective length of NSM FRP rods or laminates (L_{ef}). L_{total} can be calculated for different scenarios as follows:

(1) If $\frac{d_{fv}}{2} < L_{ef}$:

$$L_{total} = ([n_f]-\left[\frac{n_f}{2}\right])\cdot r_f + s_f \cdot \left[\frac{n_f}{2}\right]\cdot(\left[\frac{n_f}{2}\right]+1) = (\left[\frac{n_f}{2}\right]+1)\times\ (r_f + s_f\left[\frac{n_f}{2}\right]) : [n_f] \text{ is an odd number} \quad (8)$$

$$L_{total} = ([n_f]-\left[\frac{n_f}{2}\right])\cdot r_f + s_f \cdot \left[\frac{n_f}{2}\right]^2 = \left[\frac{n_f}{2}\right]\times(r_f + s_f\left[\frac{n_f}{2}\right]) \qquad : [n_f] \text{ is an even number} \quad (9)$$

where $[n_f]$ and $\left[\frac{n_f}{2}\right]$ are the integer parts of $\left(\frac{d_{fv}}{s_f}\right)$ and $\left(\frac{d_{fv}}{2s_f}\right)$, respectively, and $r_f = d_{fv} - s_f [n_f]$.

(2) If $\frac{d_{fv}}{2} \geq L_{ef}$:

$$L_{total} = (\frac{d_{fv}-2L_{ef}}{s_f}+1)\cdot L_{ef} + \left[\frac{n'_f}{2}\right]\times(r'_f + s_f \cdot \left[\frac{n'_f}{2}\right]) \quad (10)$$

where $[n'_f]$ and $\left[\frac{n'_f}{2}\right]$ are the integer parts of $\left(\frac{2L_{ef}}{s_f}\right)$ and $\left(\frac{L_{ef}}{s_f}\right)$, respectively, and $r'_f = 2L_{ef} - s_f \cdot [n'_f]$.

Consequently, the effective FRP strain corresponding to NSM FRP debonding at the concrete/epoxy interface, ($\boldsymbol{\varepsilon}_{ef-b}$), can be written as:

$$\varepsilon_{ef-b} = \frac{0.4k_{ef} \cdot \varphi_f^{\ 0.25} \cdot f_c'^{\ 0.33}\sqrt{L_{per}}}{\sqrt{E_f A_f}} \quad (11)$$

Note that the equations proposed in this paper are for vertical NSM FRP rods. The corresponding equations for inclined NSM FRP rods and laminates will be presented in a separate study by the authors.

Failure due to Concrete-Cover Splitting

Concrete-cover splitting at the RC beam's web for specimens shear-strengthened with NSM FRP occurs entirely in the concrete when the stresses in the failure zone reach the concrete tensile strength. This failure mode can be expected more often in specimens with weak concrete and tightly spaced NSM FRP. In an experimental study to investigate the bond behaviour of NSM FRP laminates bonded to concrete blocks, Seo *et al.* (2012) proposed a concrete-cover splitting model for grouped NSM FRP bonded to concrete. According to their model, the concrete splitting capacity for NSM FRP laminates bonded to concrete blocks (P_{fc}) can be calculated as follows:

$$P_{fc} = 0.57\beta\sqrt{f_c'}A_{cf} \tag{12}$$

Where f_c', β, and A_{cf} are respectively the compressive strength of concrete in MPa, an experimental coefficient equal to 0.7, and the surface area of splitting failure of concrete in mm^2. Seo *et al.* (2012) proposed an equation to calculate the concrete surface area of splitting failure for one NSM FRP laminate as follows:

$$A_{cf} = 2w_f\sqrt{L_{mb}^2 + b_{e1}^2} + L_{mb}(t_f + b_{e1}) \tag{13}$$

where w_f, t_f, L_{mb}, and b_{e1}, are the width, thickness, embedment length of FRP laminates and b_{e1} is taken equal to $0.3L_{mb}$. In this study, A_{cf} is modified to consider the effect of all active NSM FRP rods or laminates in concrete cover splitting failure for RC beams strengthened in shear with NSM FRP as follows:

$$A_{cf} = L_{total}(2w_f + 0.3L_{mb} + t_f) \qquad \text{for FRP plates} \tag{14}$$

$$A_{cf} = L_{total}(3D_f + 0.3L_{mb}) \qquad \text{for FRP rods} \tag{15}$$

where the embedment length can be taken equal to minimum of L_{eff} and $\left(\frac{d_{fv}}{2\sin\alpha}\right)$. Hence, the concrete-cover splitting force can be used to calculate the FRP effective strain corresponding to the concrete-cover splitting failure mode as follows:

$$\varepsilon_{fe-c} = \frac{0.4\sqrt{f_c'}A_{cf} \cdot s_f}{A_f \cdot E_f \cdot d_f} \tag{16}$$

Note that the effective strain in the NSM FRP rods or laminates at ultimate load can be taken as the minimum of the strain due to NSM FRP debonding at the split between the concrete/epoxy interface and the concrete cover, i.e.,

$$\varepsilon_{fe} = \min(\varepsilon_{fe-b}, \varepsilon_{fe-c}) \tag{17}$$

Verification of the proposed design equations

The experimental contributions of FRP to shear resistance of the retrofitted specimens in this study are compared with the shear resistance predicted by the proposed equations (Table 4). The calculated values of effective strain developed in the NSM FRP rods corresponding to each failure mode are shown in Table 4. The governing failure mode can thus be identified. The FRP shear contribution is then calculated based on the critical effective strain of the governing failure mode. Finally, the experimental results of this study are compared to the results calculated using the proposed equations (Table 4). For specimens NR-NSM and MR-NSM, the governing shear failure mode according to the calculation is concrete-cover splitting, where the calculated FRP shear contribution ($V_{f\text{-}g}$) for these specimens was 47.8 and 52.0 kN respectively. The experimental FRP shear contribution for these two specimens is 49.8 and 56.9 kN respectively, resulting in a calculated V_f to experimental V_f ratios of 0.96 and 0.91 respectively. This indicates a fairly accurate and conservative prediction by the proposed equations compared with experimental results.

To further assess the validity of the proposed theoretical predictions, test results from the database are also used (Table 3). The 69 specimens presented in Table 3 all failed due to debonding of NSM FRP or concrete cover splitting (the results of specimens failed with no major contribution of NSM FRP to the shear resistance, those of specimens failed due to unrelated failure modes to the shear resistance, and those of specimens with special anchorage of NSM FRP is not presented here). The accuracy of the predicted contributions of FRP to the shear resistance by the proposed model is compared to that of the existing design equations in literature proposed by De Lorenzis and Nanni (2001), Kotynia (2007), Anwarul Islam (2009), and Dias and Barros (2013). Figures 11(a) to 11(e) show the $V_{f\ cal}$ values calculated using the proposed model and each of the existing design models versus the experimental values of $V_{f\ exp.}$ The results of this study show that the proposed model's accuracy (R^2 = 0.55) is superior to the existing design models [Fig. 11(a)]. The proposed model can calculate the shear contribution of FRP for both beams strengthened with rods and laminates with high accuracy (R^2 = 0.58 and R^2 = 0.53, respectively, when FRP rods and laminates are considered separately). The predicted results by De Lorenzis and Nanni (2001) for NSM FRP rods show reasonable accuracy with the experimental results (R^2 = 0.34) [Fig. 11(b)]. However, the modified version by Parretti and Nanni (2004) to make the model applicable to NSM FRP laminates does not show good correlation with experimental results (R^2 = 0.15, the results are not included in Table 3). This could be due to the fact that the model is not originally calibrated for NSM FRP laminates. The results produced by Kotynia (2007) and Anwarul Islam (2009) [Fig. 11(c)] do not show a great correlation with experimental results in database (R^2 < 0.1). Dias and Barros (2013) model (applicable to NSM FRP laminates) predicts V_f with reasonable accuracy when compared to experimental results of RC beams strengthened with NSM laminates (R^2 = 0.44) [Fig. 11(d)]. However, when the experimental results directly used by the researchers to calibrate their model are removed, the accuracy of Dias and Barros (2013) model drops significantly (R^2 < 0.1) [Fig. 11(e)]. This could be due to the fact that their model considers the diminishing effect of steel stirrups on NSM FRP contribution to the shear resistance, which the experimental results analysed in this study shows is not as significant as it was observed previously for EB FRP.

The predicted results of the models are also compared with respect to the ratio of $(V_{f\,cal})/(V_{f\,exp})$. The proposed model and De Lorenzis and Nanni (2001) model produce accurate and conservative values with respect to $(V_{f\,cal})/(V_{f\,exp})$ ratio (0.89 and 0.90 respectively). Whereas, models by Dias and Barros (2013) and Anwarul Islam (2009) produce non-conservative predictions with $(V_{f\,cal})/(V_{f\,exp})$ equal to 1.17 and 1.91, respectively.

It should be noted that the proposed model is currently the only design model that can predict the failure mode of the shear strengthened beams with NSM FRP. When compared to the experimental results in the database, the proposed model was able to predict the failure mode of the beams with reasonable accuracy, i.e., 84% and 65% correct predicted failure modes for debonding and concrete covered splitting failure modes respectively.

CONCLUSIONS

This paper presents the results of an experimental investigation involving six tests on RC T-beams strengthened in shear using near-surface mounted FRP rods. The parameters of the experimental part of this study were: (i) the effectiveness of the NSM FRP rods, (ii) the presence of steel stirrups, and (iii) the steel stirrup ratio. This paper has provided an insightful and broad description of the behaviour of RC beams strengthened in shear with NSM FRP under increasing load. The behaviour of FRP and of steel stirrups has been analyzed in depth, in particular at ultimate stage within the failure zone. The results of this study and those gathered in a database were further used to verify a newly proposed model to predict the shear contribution of RC beams strengthened with NSM FRP. The main findings of this research can be stated as follows:

- The near-surface mounting method greatly enhanced the overall behaviour of RC beams because the strengthened beams showed higher load at failure (31% on average) and greater maximum deflection than their corresponding control specimens.
- Proper NSM strengthening led to formation of concrete struts throughout the shear span of the RC beams, resulting in a distributed crack pattern. Unlike the control specimens, in the strengthened beams the first shear crack that caused the first steel stirrup to yield was not necessarily the principal shear crack that led to ultimate shear failure.
- The experimental results of this study and those presented in the database have revealed that the presence of steel stirrups did not diminish the NSM FRP shear contribution. This might have been due to the fact that the highly stressed areas around the existing steel stirrups and the FRP did not normally overlap in the NSM strengthening method.
- Yielding of steel stirrups were observed in all specimens tested in this study, as generally assumed in the design models for RC beams with steel stirrups strengthened in shear with FRP (e.g., ACI 440.2R-08 and CSA/S806-12).
- The proposed design model shows good correlation between the predicted results and the experimental results presented in the database as well as other available design models in literature. The proposed model produces accurate and conservative values with $(V_{f\,cal})/(V_{f\,exp})$ equal to 0.89. This new design model is also the only model that can reasonably

predict the possible failure modes of strengthened RC beams using NSM FRP rods and laminates.

ACKNOWLEDGMENTS

The authors acknowledge the support provided by Mitacs and Sika Canada Inc. through a Mitacs postdoctoral fellowship to Dr. Mofidi, by the Natural Sciences and Engineering Research Council of Canada through a Discovery grant to Prof. Chaallal and by the University of California, Davis, for partial financial support of the research. The authors thank Mr. Philippe Guevremont and Mr. Bob Barham at Sika Canada Inc. for their contributions to this research. The efficient collaboration of John Lescelleur (senior technician) at ÉTS, in conducting the tests, is acknowledged.

REFERENCES

ACI 318-11 (2011). *Building Code Requirements for Structural Concrete*, American Concrete Institute (ACI), Farmington Hills MI.

Asplund, S.O (1949) Strengthening bridge slabs with grouted reinforcement. *ACI Struct J* 20(5), 397–406.

American Concrete Institute (ACI) (2008). *Guide for the Design and Construction of Externally Bonded FRP Systems for Strengthening Concrete Structures.* Report No. 440 2R-08, Farmington Hills MI.

Anwarul Islam, A.K.M. (2009). Effective methods of using CFRP bars in shear strengthening of concrete girders. *Eng. Struct.* 31, 709–714.

Blaschko, M. (2003). Bond behavior of CFRP strips glued into slits. *Proceedings, 6th International Symposium on Fiber-Reinforced Polymer Reinforcement for Concrete Structures*, K.H. Tan (ed.), Singapore, 205–214.

Blaschko, M. and Zilch, K. (1999). Rehabilitation of concrete structures with CFRP strips glued into slits. *Proc. of the 12th Int. Conf. on Compos Mater*. Paris. July 5-9.

Bilotta, A., Ceroni, F., Di Ludovico, M., Nigro, E., Pecce, M., and Manfredi, G. (2011). Bond efficiency of EBR and NSM FRP systems for strengthening concrete members. *J. Compos. Constr.* 15(5), 757-772.

Barros, J.A.O., and Dias, S.J.E. (2006). Near-surface mounted CFRP laminates for shear strengthening of concrete beams. *Cem. Concr. Compos.* 28, 276–292.

CAN/CSA-A23.3 (2014). *Design of Concrete Structures*. Canadian Standards Association, Rexdale, Canada.

CAN/CSA-S806-12 (2012). *Design and construction of building components with fiber-reinforced polymer.* Canadian Standards Association, Rexdale, Canada.

Chaallal, O., Mofidi, A., Benmokrane, B., and Neale, K. (2011). Embedded through-section FRP rod method for shear strengthening of RC beams: performance and comparison with existing techniques. *J. Compos. Constr.* 15(3), 374-383.

Cisneros, D., Arteaga, A., De Diego, A., and Alzate, A. (2012). Experimental study on NSM FRP shear retrofitting of RC beams. *Proc. of the 6th Int. Conf. on FRP Compos. in Civil Eng.* University of Roma, Rome, Italy.

Dias, S.J.E., and Barros, J.A.O. (2008). Shear strengthening of T-cross section reinforced concrete beams by near-surface mounted technique. *J. Compos. Constr.* 12(3), 300–311.

Dias, S.J.E., and Barros, J.A.O. (2010). Performance of reinforced-concrete T-beams strengthened in shear with NSM CFRP laminates. *Eng. Struct.* 32, 373–384.

Dias, S.J.E., and Barros, J.A.O. (2011). Shear strengthening of RC T-section beams with low-strength concrete using NSM CFRP laminates. *Cem. Concr. Compos.* 33, 334–345.

Dias, S.J.E., and Barros, J.A.O. (2012). NSM shear-strengthening technique with CFRP laminates applied in high-strength concrete beams with or without pre-cracking. *Composites: Part B.* 43, 290–301.

Dias, S.J.E., and Barros, J.A.O. (2013). Shear strengthening of RC beams with NSM CFRP laminates: Experimental research and analytical formulation. *Compos. Struct.* 99, 477-490.

De Lorenzis, L. (2004). Anchorage length of near-surface mounted fiber-reinforced polymer rods for concrete strengthening-analytical modeling. *ACI Struct. J.* 101(3), 375–384.

De Lorenzis, L. and Nanni, A. (2001). Shear-strengthening of reinforced concrete beams with NSM fibre-reinforced polymer rods. *ACI Struct. J.* 98(1), 60–68.

Galal, K. and Mofidi, A. (2010). Shear-strengthening of RC T-beams using mechanically anchored unbonded dry carbon fibre sheets. *J. Performance Constructed Facilities* 24(1), 31–39.

Jalali, M., Sharbatdar, M.K., Chen, J.F., and Jandaghi Alaee, F. (2012). Shear strengthening of RC beams using innovative manually made NSM FRP bars. *Constr. Build Mater.* 36, 990–1000.

Kotynia, R. (2007). Shear strengthening of RC beams with NSM CFRP laminates. *Proc. of the 8th symposium of fibre-reinforced polymers in reinforced concrete structures*, University of Patras, Patras, Greece.

Mofidi, A. and Chaallal, O. (2011). Shear Strengthening of RC Beams with Epoxy Bonded FRP—Influencing Factors and Conceptual Debonding Model. American Society of Civil Engineers, *J. Compos. Constr.* 15(1), 62-74.

Mofidi, A., Chaallal, O., Benmokrane, B., and Neale, K.W. (2012a). Experimental tests and design model for RC beams strengthened in shear using the embedded through-section FRP method. *J. Compos. Constr.* 16(5), 540–550.

Mofidi, A., Chaallal, O., Benmokrane, B., and Neale, K.W. (2012b). Performance of end-anchorage systems for RC beams strengthened in shear with epoxy-bonded FRP. *J. Compos. Constr.* 16(3), 322–331.

Mofidi, A. and Chaallal, O. (2014a). Effect of Steel Stirrups on the Shear Resistance Gain Due to EB FRP Strips and Sheets. *ACI Struct. J.* 111(2), 353-362.

Mofidi, A. and Chaallal, O. (2014b). Tests and Design Provisions for Reinforced-Concrete Beams Strengthened in Shear using FRP Sheets and Strips. *Int. J. Concr. Struct. Mater.* 8(2), 117-128.

Nanni, A., Alkhrdaji, T., Barker, M., Chen, G., Mayo, R., and Yang, X. (1999) Overview of testing to failure program of a highway bridge strengthened with FRP composites. *Proc of the Fourth Int Symp on Non-Metallic (FRP) Reinforcement for Concrete Structures (FRPRCS-4)*, SP-188, American Concrete Institute, Farmington Hills. MI, 69–75.

Parretti, R. and Nanni, A. (2004). Strengthening of RC members using Near-Surface Mounted FRP composites: design overview. *Advanc. Struct. Eng.* 7(5), 1-16.

Pellegrino, C., and Vasic, M. (2013). Assessment of design procedures for the use of externally bonded FRP composites in shear strengthening of reinforced concrete beams. *Compos. Part B: Eng.* 45(1), 727-741.

Rahal, K.N. and Rumaih, H.A. (2011). Tests on reinforced concrete beams strengthened in shear using near surface mounted CFRP and steel bars. *Eng. Struct.* 33, 53–62.

Raj, S.D. and Surumi, R.S. (2012). Shear strengthening of reinforced concrete beams using near surface mounted glass fibre reinforced polymer. *Asian J. of Civil Eng. (Building and housing)* 13(5), 679–690.

Rizzo, A. and De Lorenzis, L. (2007). Behavior and capacity of RC beams strengthened in shear with NSM FRP reinforcement. *Constr. Build Mater.* 23, 1555-1567.

Seo, S.Y., Feo, L., and Hui, D. (2012). Bond strength of near surface-mounted FRP plate for retrofit of concrete structures. *Compos. Struct.* 95, 719-727.

Seracino, R., Jones, N.M., Ali, M.S.M., Page, M.W., and Oehlers, D.J. (2007a). Bond strength of near-surface mounted FRP strip-to-concrete joints. *J. Compos. Constr.* 11(4), 401–409.

Seracino, R., Raizal Saifulnaz, M.R., and Oehlers, D.J. (2007b). Generic debonding resistance of EB and NSM plate-to-concrete joints. *J. Compos. Constr.* 11(1), 62–70.

Wiwatrojanagul, P., Ayudhya, B.I.N. and Sahamitmongkol, R. (2012). NSM FRP shear strengthening of RC beams with internal stirrups. *Thammasat Int. J. of Scien. and Tech.* 17(1), 16–30.

Table 1: Description of the test specimens.

Specimen	Strengthening configuration	Internal transverse steel shear reinforcement		NSM FRP rods	
		Spacing (mm)	Diameter (mm)	Spacing (mm)	Diameter (mm)
NR-CON	-*	-	-	-	-
MR-CON	-	260	8	-	-
HR-CON	-	175	8	-	-
NR-NSM	NSM rods	-	-	130	9.5
MR-NSM	NSM rods	260	8	130	9.5
HR-NSM	NSM rods	175	8	130	9.5

*Not applicable.

Table 2: Experimental results.

Specimen	Load at rupture (kN)	Total shear resistance (kN)	Resistance due to concrete (kN)	Resistance due to steel (kN)	Resistance due to CFRP (kN)	Gain due to CFRP (%)	Deflection at load point (mm)	Failure mode*
NR-CON	122.7	81.3	81.3	0.0	0.0	0	2.6	DTF
MR-CON	294.0	194.7	88.5	106.2	0.0	0	11.2	DTF
HR-CON	350.6	232.2	81.3	150.9	0.0	0	11.9	DTF
NR-NSM	198.0	131.1	81.3	0.0	49.8	61	6.1	CCS
MR-NSM	380.0	251.6	88.5	106.2	56.9	29	11.7	CCS/FLX
HR-NSM	365.0	241.7	81.3	150.9	9.5	4	13.1	FLX/CCS

*Note: DTF, CCS and FLX correspond to diagonal tension, concrete cover splitting and flexural failure modes.

Table 3: Experimental data of shear strengthening using NSM FRP.

Specimen	b_w (mm)	d (mm)	f'_c (MPa)	FRP shape	ρ_f (%)	ρ_{sv} (%)	E_f (GPa)	ε_{fu}^* ($\times 10^{-3}$)	α (°)	$V_{f\,cal}$ DN (kN)	$V_{f\,cal}$ KT (kN)	$V_{f\,cal}$ AN (kN)	$V_{f\,cal}$ DB (kN)	$V_{f\,cal}$ Proposed (kN)	$V_{f\,exp}$ (kN)
DN(B45-7)	152	356	31	Rods	0.74	0.00	105	18	45	67.9	119.1	177.2	n/a	108.7	75.1
DN(B90-5)	152	356	31	Rods	0.73	0.00	105	18	90	32.1	118.1	248.4	n/a	48.7	37.4
DN(B90-7)	152	356	31	Rods	0.52	0.00	105	18	90	11.1	84.2	177.2	n/a	25.6	24.9
BD(B10-VL)	150	123	56	Strips	0.19	0.00	150	14	90	n/a	14.6	25.3	47.0	1.22	28.6
BD(B10-IL)	150	123	56	Strips	0.18	0.00	150	14	45	n/a	13.8	16.8	89.0	5.4	23.2
BD(B12-VL)	150	123	56	Strips	0.37	0.00	150	14	90	n/a	29.3	50.5	59.0	12.6	31.8
BD(B12-IL)	150	123	56	Strips	0.35	0.00	150	14	45	n/a	27.6	33.7	82.0	22.2	36.4
DB(2S-3LV-a)	180	356	31	Strips	0.06	0.10	167	18	90	n/a	17.6	36.7	28.2	4.8	0.6
DB(2S-5LV-a)	180	356	31	Strips	0.10	0.10	167	18	90	n/a	29.4	61.3	41.4	24.0	25.2
DB(2S-8LV-a)	180	356	31	Strips	0.16	0.10	167	18	90	n/a	47.1	98.1	56.6	49.6	48.6
DB(2S-5LI45-a)	180	356	31	Strips	0.10	0.10	167	18	45	n/a	30.3	44.6	58.4	78.4	41.4
DB(2S-8LI45-a)	180	356	31	Strips	0.16	0.10	167	18	45	n/a	48.2	71.1	71.7	75.6	40.2
DB(2S-3LI60-a)	180	356	31	Strips	0.06	0.10	167	18	60	n/a	19.8	30.2	42.1	13.3	35.4
DB(2S-5LI60-a)	180	356	31	Strips	0.09	0.10	167	18	60	n/a	33.0	50.3	57.2	38.0	46.2
DB(2S-7LI60-a)	180	356	31	Strips	0.13	0.10	167	18	60	n/a	46.3	70.6	67.5	78.2	54.6
RD(NB45-73-a)	200	173	29	Rods	0.97	0.18	146	15	45	70.1	139.1	175.8	n/a	38.5	28.0
RD(NB90-45-b)	200	173	29	Rods	1.12	0.18	146	15	90	48.6	159.6	285.2	n/a	16.0	28.6
RD(NB90-73-b)	200	173	29	Rods	0.69	0.18	146	15	90	30.2	98.4	175.8	n/a	16.0	26.4
RD(NB90-73-a)	200	173	29	Rods	0.69	0.18	146	15	90	30.2	98.4	175.8	n/a	16.0	54.2
RD(NB45-146-a)	200	173	29	Rods	0.48	0.18	146	15	45	35.0	69.6	87.9	n/a	16.7	39.1
RD(NS90-73-a)	200	173	29	Strips	0.44	0.18	122	17	90	n/a	52.2	104.6	53.6	18.6	50.5
RD(NS45-146-a)	200	173	29	Strips	0.31	0.18	122	17	45	n/a	37.0	52.3	41.0	18.6	32.7
JL(VR)	200	214	36	Rods	0.09	0.19	235	15	90	17.3	128.0	248.5	n/a	6.5	33.4
JL(IR)	200	214	36	Rods	0.09	0.19	235	15	45	27.6	120.7	165.7	n/a	19.3	39.9
DB(3S-10LV-d)	180	360	59	Strips	0.13	0.10	174	16	90	n/a	41.5	79.7	69.3	65.8	65.9
DB(3S-5LI45-d)	180	360	59	Strips	0.08	0.10	174	16	45	n/a	24.3	33.0	83.6	67.6	66.1
DB(3S-5LI45F1-d)	180	360	59	Strips	0.08	0.10	174	16	45	n/a	24.3	33.0	83.6	67.6	85.8
DB(3S-5LI45F2-d)	180	360	59	Strips	0.08	0.10	174	16	45	n/a	24.3	33.0	83.6	67.6	65.4
DB(3S-9LI45-d)	180	360	59	Strips	0.13	0.10	174	16	45	n/a	42.6	57.9	110.1	107.0	101.9
DB(3S-8LI60-d)	180	360	59	Strips	0.11	0.10	174	16	60	n/a	39.9	56.1	100.1	103.3	112.3
DB(5S-5LI45-d)	180	360	59	Strips	0.08	0.16	174	16	45	n/a	24.3	33.0	62.0	67.6	74.9
DB(5S-5LI45F-d)	180	360	59	Strips	0.08	0.16	174	16	45	n/a	24.3	33.0	62.0	67.6	101.1
DB(5S-9LI45-d)	180	360	59	Strips	0.13	0.16	174	16	45	n/a	42.6	57.9	86.8	107	108.9
DB(5S-5LI60-d)	180	360	59	Strips	0.07	0.16	174	16	60	n/a	26.6	37.4	59.9	60.6	73.4
DB(5S-5LI60F-d)	180	360	59	Strips	0.07	0.16	174	16	60	n/a	26.6	37.4	59.9	60.6	72.6

Table 3: Experimental data of shear strengthening using NSM FRP (cont'd).

DB(5S-8LI60-d)	180	360	59	Strips	0.11	0.16	174	16	60	n/a	39.9	56.1	77.7	103.4	122.5
DB(2S-4LV-b)	180	360	40	Strips	0.08	0.10	171	16	90	n/a	25.8	48.6	41.6	22.0	20.2
DB(2S-7LV-b)	180	360	40	Strips	0.13	0.10	171	16	90	n/a	40.7	76.8	57.1	50.6	42.1
DB(2S-10LV-b)	180	360	40	Strips	0.18	0.10	171	16	90	n/a	58.0	109.4	71.2	56.3	56.2
DB(2S-4LI45-b)	180	360	40	Strips	0.08	0.10	171	16	45	n/a	23.9	31.8	61.2	59.5	53.4
DB(2S-7LI45-b)	180	360	40	Strips	0.13	0.10	171	16	45	n/a	41.8	55.7	80.9	107.8	70.7
DB(2S-10LI45-b)	180	360	40	Strips	0.19	0.10	171	16	45	n/a	59.6	79.6	92.2	107.8	85.6
DB(2S-4LI60-b)	180	360	40	Strips	0.07	0.10	171	16	60	n/a	26.1	36.0	59.5	30.3	49.6
DB(2S-6LI60-b)	180	360	40	Strips	0.11	0.10	171	16	60	n/a	39.1	54.0	74.3	63.3	54.4
DB(2S-9LI60-b)	180	360	40	Strips	0.16	0.10	171	16	60	n/a	58.7	81.0	88.6	98.6	65.3
DB(2S-7LV-c)	180	360	19	Strips	0.13	0.10	174	16	90	n/a	41.5	79.7	41.1	31.7	28.3
DB(2S-4LI45-c)	180	360	19	Strips	0.08	0.10	174	16	45	n/a	24.3	33.1	35.2	23.3	33.9
DB(2S-7LI45-c)	180	360	19	Strips	0.13	0.10	174	16	45	n/a	42.6	57.9	46.4	73.1	48.0
DB(2S-4LI60-c)	180	360	19	Strips	0.07	0.10	174	16	60	n/a	26.6	37.4	34.5	19.0	33.1
DB(2S-6LI60-c)	180	360	19	Strips	0.11	0.10	174	16	60	n/a	39.9	56.1	43.0	39.7	42.7
DB(4S-7LV-c)	180	360	19	Strips	0.13	0.17	174	16	90	n/a	41.5	79.7	34.1	31.7	6.8
DB(4S-4LI45-c)	180	360	19	Strips	0.08	0.17	174	16	45	n/a	24.3	33.1	24.0	23.3	26.0
DB(4S-7LI45-c)	180	360	19	Strips	0.13	0.17	174	16	45	n/a	42.6	57.9	34.1	73.1	31.7
DB(4S-4LI60-c)	180	360	19	Strips	0.07	0.17	174	16	60	n/a	26.6	37.4	23.4	19.0	25.2
DB(4S-6LI60-c)	180	360	19	Strips	0.11	0.17	174	16	60	n/a	39.9	56.1	30.7	39.7	35.2
RR(B2)	150	430	44	Rods	0.34	0.19	124	15	90	34.7	76.0	137.0	n/a	37.9	70.0
RR(B4)	150	430	44	Rods	0.47	0.19	124	15	45	72.7	107.5	137.0	n/a	152.1	138.0
KT(BI-2/3B)	150	310	39	Strips	0.19	0.19	163	14	45	n/a	40.5	46.5	54.5	23.8	64.6
KT(BI-3/5A)	150	310	39	Strips	0.32	0.19	163	14	45	n/a	69.5	79.7	67.8	71.0	100.6
WA(A75-90)	250	234	39	Rods	1.57	0.15	69	16	90	74.1	183.0	336.3	n/a	39.6	45.5
WA(A300-45)	250	234	39	Rods	0.55	0.15	69	16	45	12.4	64.7	84.1	n/a	12.4	43.9
WA(C75-90)	250	234	39	Rods	0.50	0.15	72	13	90	42.0	61.9	244.9	n/a	30.0	47.5
WA(C150-90)	250	234	39	Rods	0.25	0.15	72	13	90	17.0	30.4	122.5	n/a	7.6	43.8
WA(C300-45)	250	234	39	Rods	0.18	0.15	72	13	45	7.6	21.9	61.2	n/a	7.6	33.7
RS(BR90E)	175	211	35	Rods	0.32	0.00	45	19	90	8.0	15.2	35.8	n/a	8.0	36.8
RS(BR45E)	175	211	35	Rods	0.46	0.00	45	19	45	31.9	21.5	35.8	n/a	31.8	29.4
RS(BS90E)	175	211	35	Strips	0.34	0.00	44	17	90	n/a	15.8	31.7	60.4	10.4	49.0
RS(BS90E100)	175	211	35	Strips	0.34	0.00	44	17	90	n/a	15.8	31.7	60.4	10.4	61.5
RS(BS90E75)	175	211	35	Strips	0.46	0.00	44	17	90	n/a	21.1	42.2	66.3	17.7	39.2

* ε_{fu} is the ultimate strain of the FRP.

** DN = De Lorenzis and Nanni (2001); BD = Barros and Dias (2006); DB= Dias and Barros (2008, 2010, 2011, 2012, 2013); RD = Rizzo and De Lorenzis (2007); AN = Anwarul Islam (2009); JR = Jalali *et al.* (2012); RR= Rahal and Rumaih (2011); KT= Kotynia 2007; WA = Wawatrojanagul et al. (2012); and RS = Raj and Surumi (2012).

Table 4: Comparison of predicted results versus experimental results

Specimen	$\varepsilon_{fe\text{-}b}$	$\varepsilon_{fe\text{-}c}$	$\varepsilon_{fe\text{-}g}$	$V_{f\text{-}cal}$* (kN)	$V_{f\text{-}flx}$ (kN)	$V_{f\text{-}g}$ (kN)	$V_{f\text{-}exp}$ (kN)	$V_{f\text{-}g}$ / $V_{f\text{-}exp}$
NR-NSM	0.0010	0.0009	0.0009	$\underline{47.8}$**	174.7	47.8	49.8	0.96
MR-NSM	0.0011	0.0010	0.0010	$\underline{52.0}$	81.3	52.0	56.9	0.91
HR-NSM	0.0010	0.0009	0.0009	47.8	$\underline{23.8}$	23.8	9.5	2.50

* $V_{f\text{-}cal}$, $V_{f\text{-}flx}$, $V_{f\text{-}exp}$ are the FRP shear contributions corresponding to the calculated governing effective strain at ultimate load, the calculated values at flexural failure of the beam, and experimental results respectively, $V_{f\text{-}g}$ is the governing calculated shear contribution of FRP and $\varepsilon_{fe\text{-}b}$, $\varepsilon_{fe\text{-}c}$, $\varepsilon_{fe\text{-}g}$ are the corresponding effective strain to debonding and concrete cover splitting and the governing effective strain to calculate the shear contribution of FRP respectively.

** The shear contribution of FRP corresponding to the governing calculated failure mode is underlined (shear versus flexure failure modes).

Figure 1

Click here to download Figure: Fig. 1.pdf

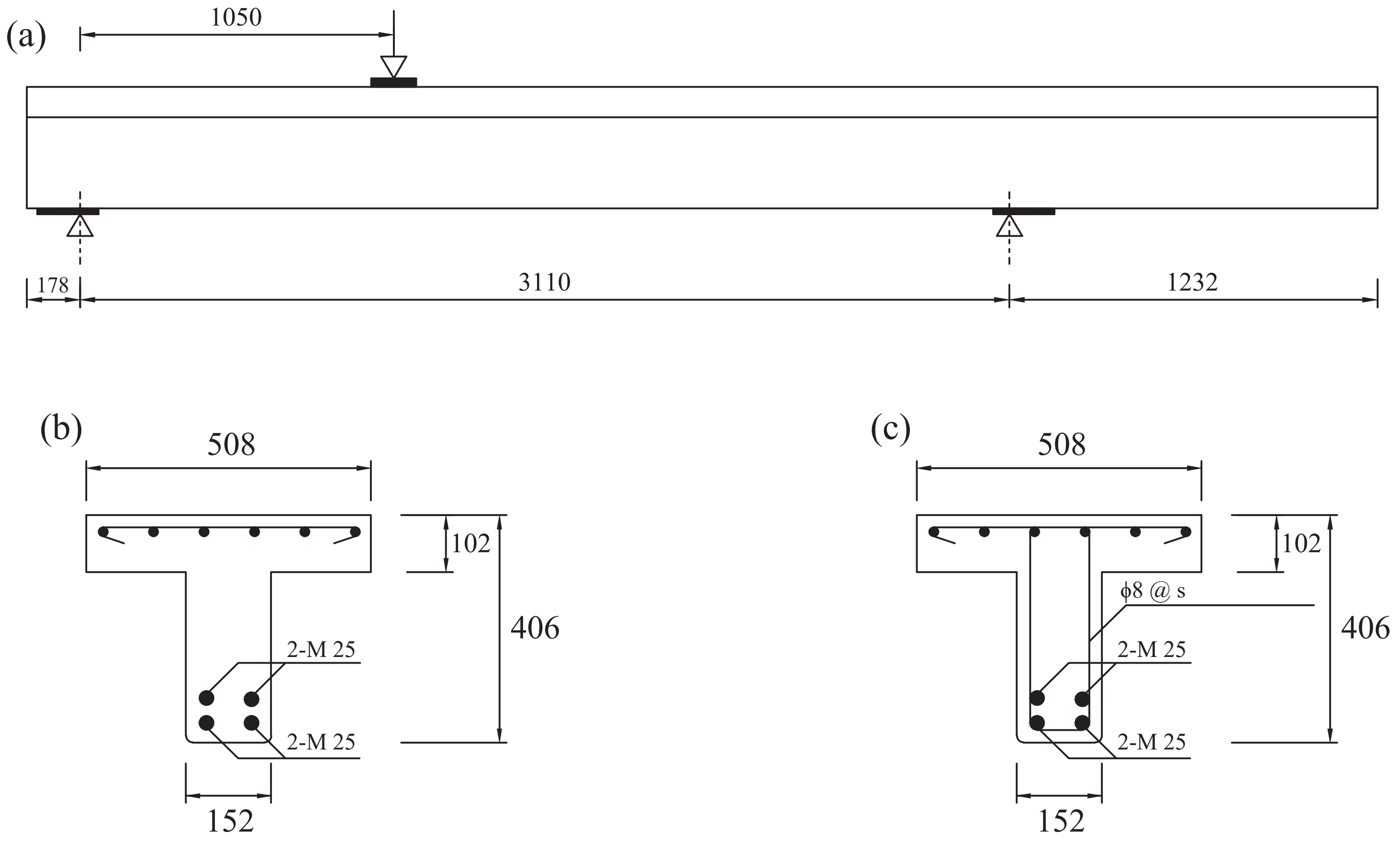

Figure 2
Click here to download Figure: Fig. 2.pdf

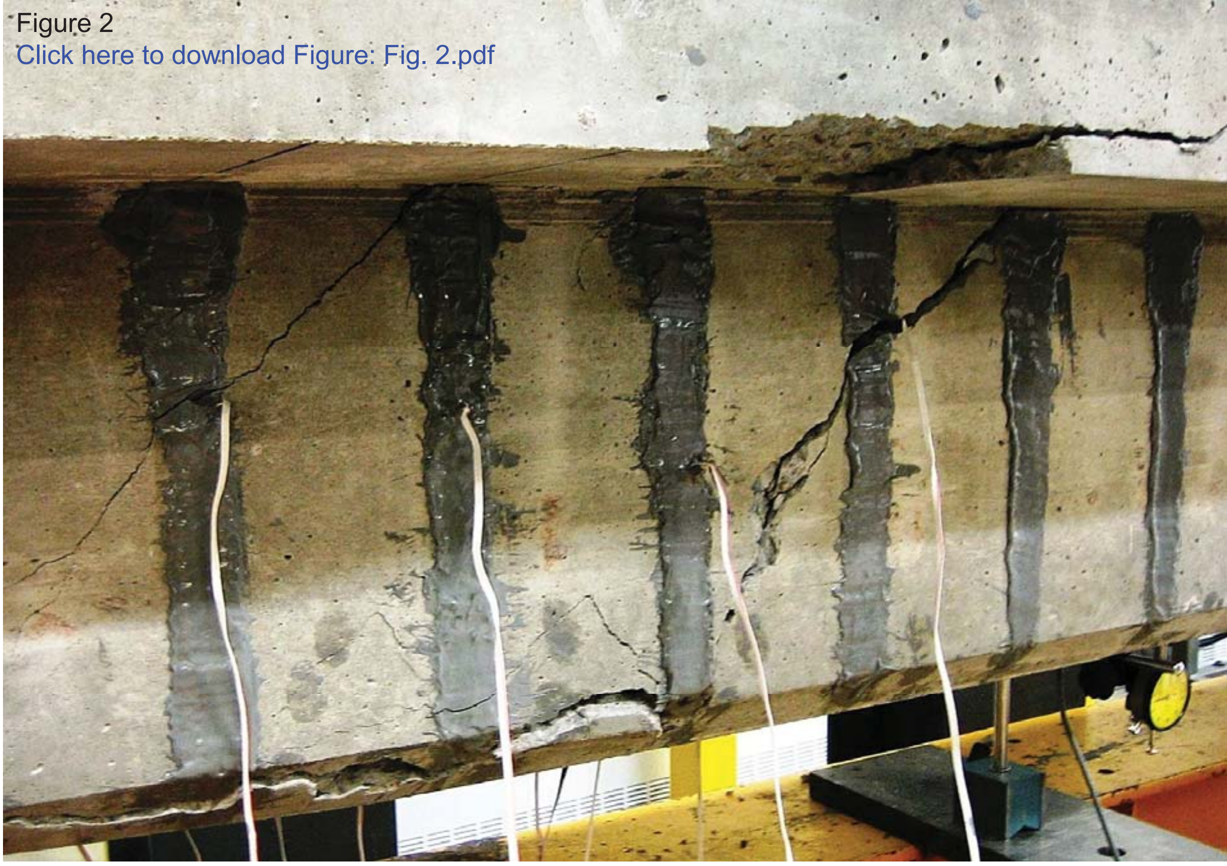

Figure 3

Click here to download Figure: Fig. 3.pdf

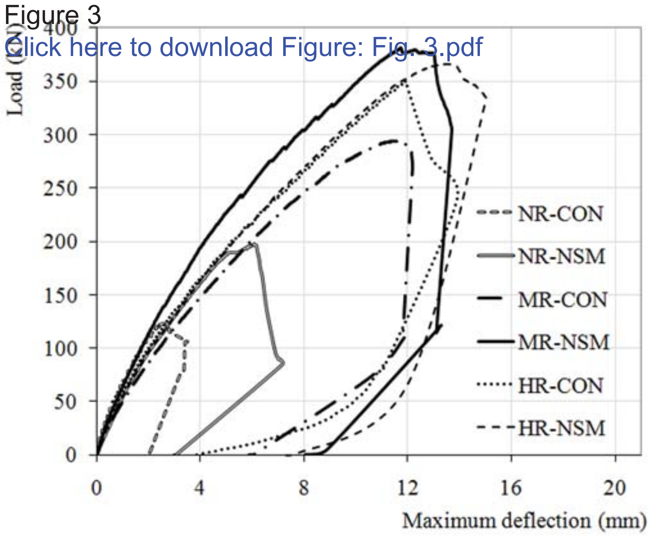

Figure 4
Click here to download Figure: Fig. 4.pdf

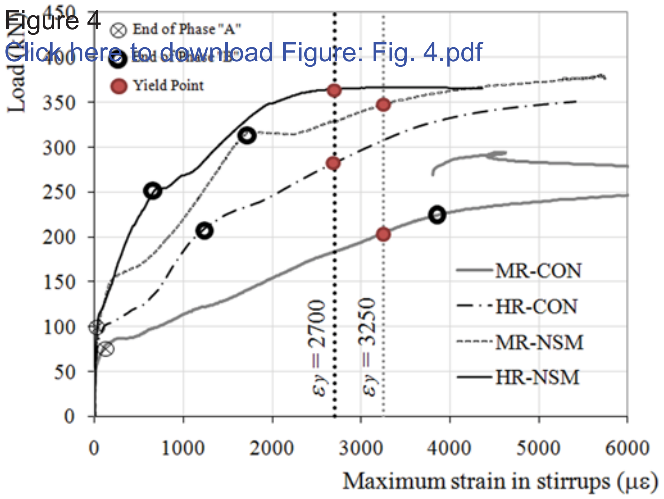

Figure 5
Click here to download Figure: Fig. 5.pdf

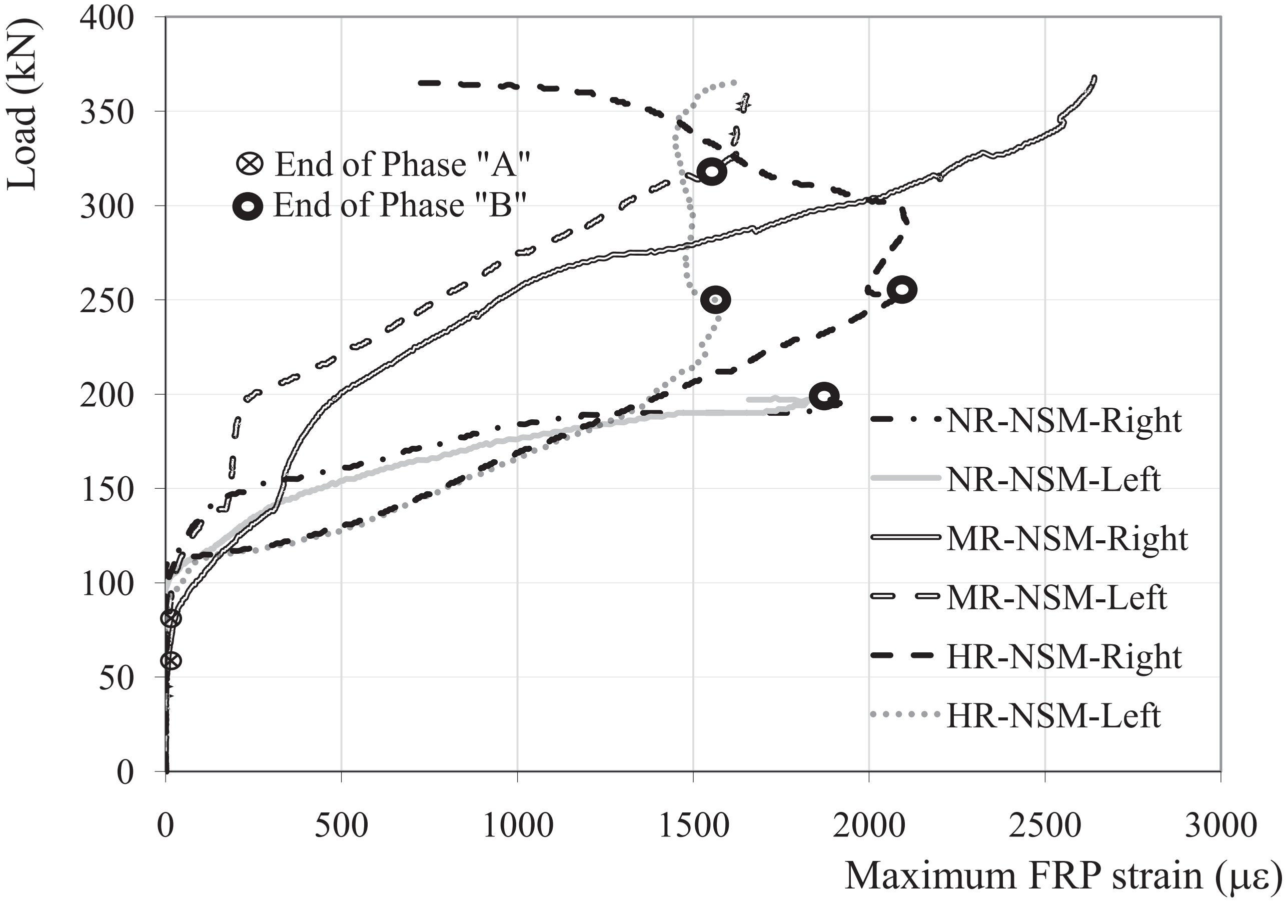

Figure 6
Click here to download Figure: Fig. 6.pdf

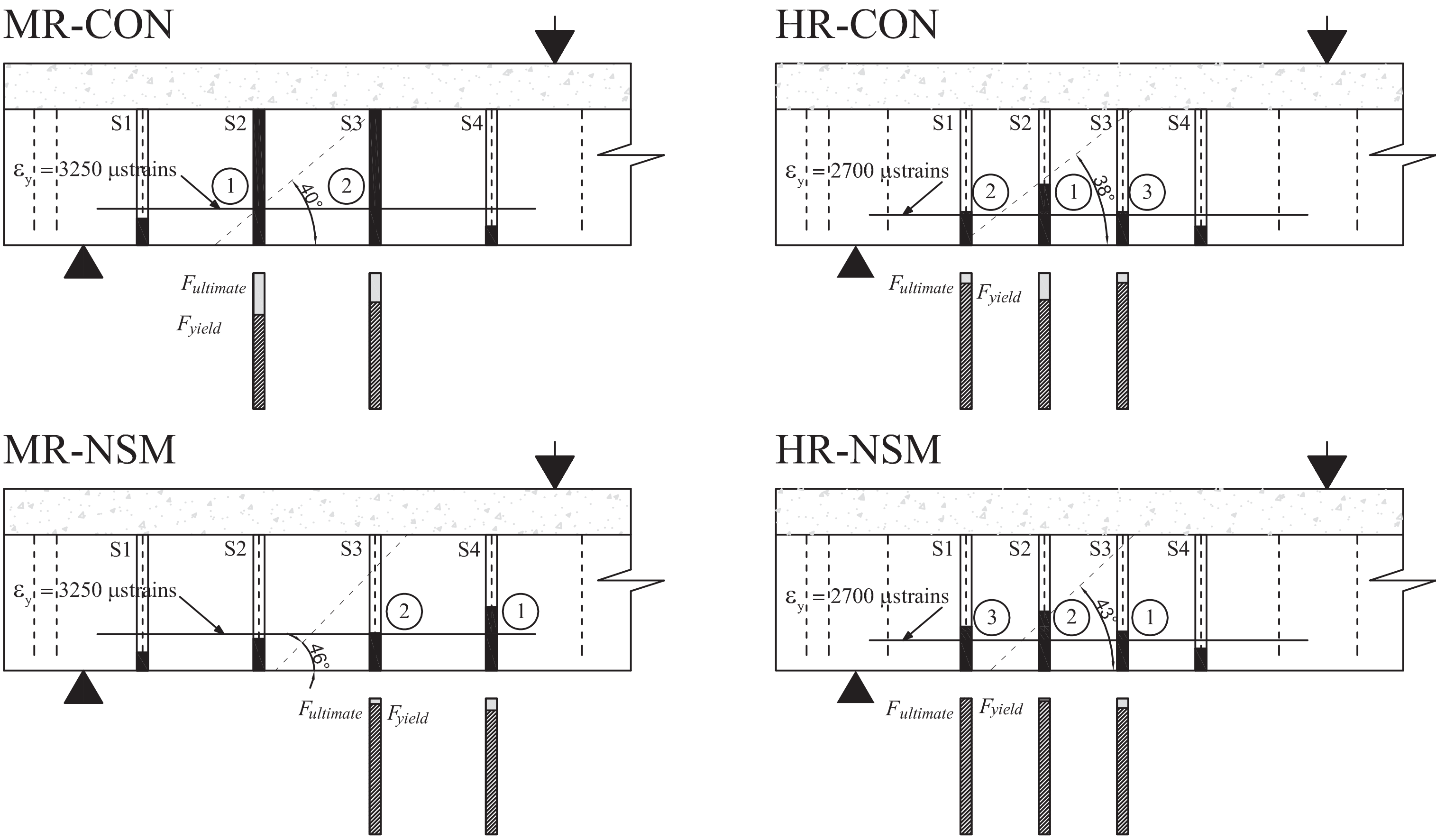

Figure 7

Click here to download Figure: Fig. 7.pdf

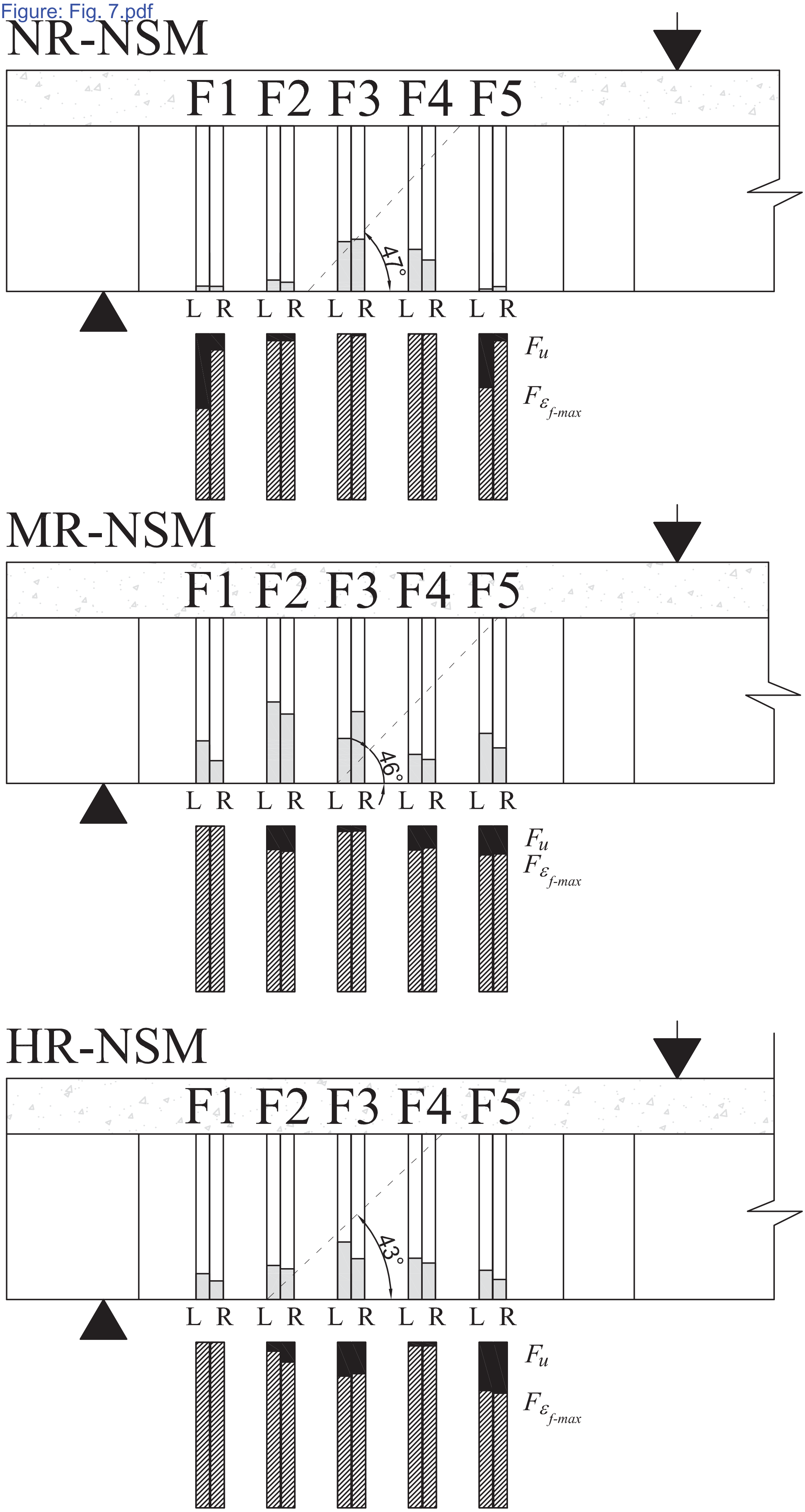

Figure 8
Click here to download Figure: Fig. 8.pdf

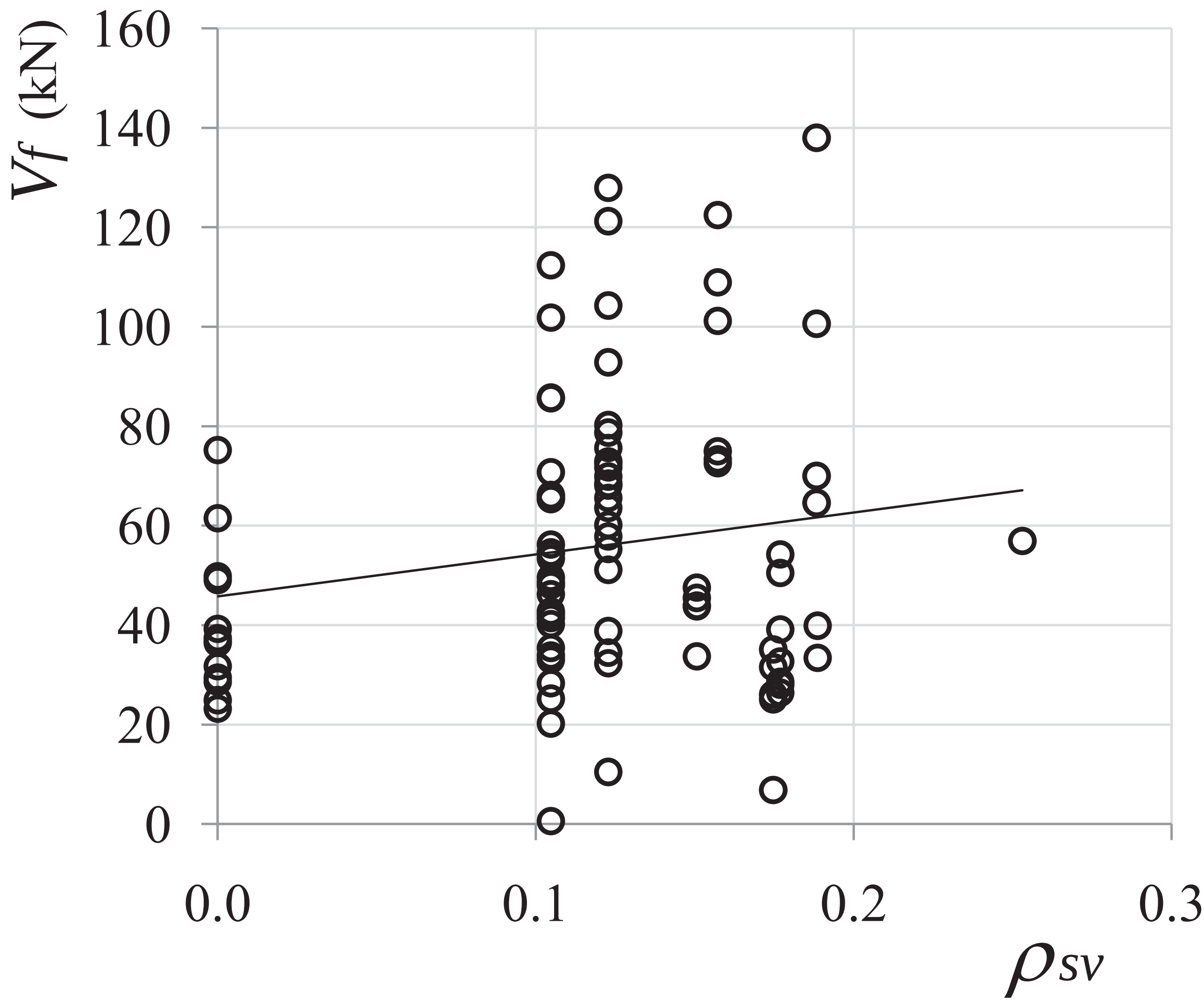

Figure 9
Click here to download Figure: Fig. 9.pdf

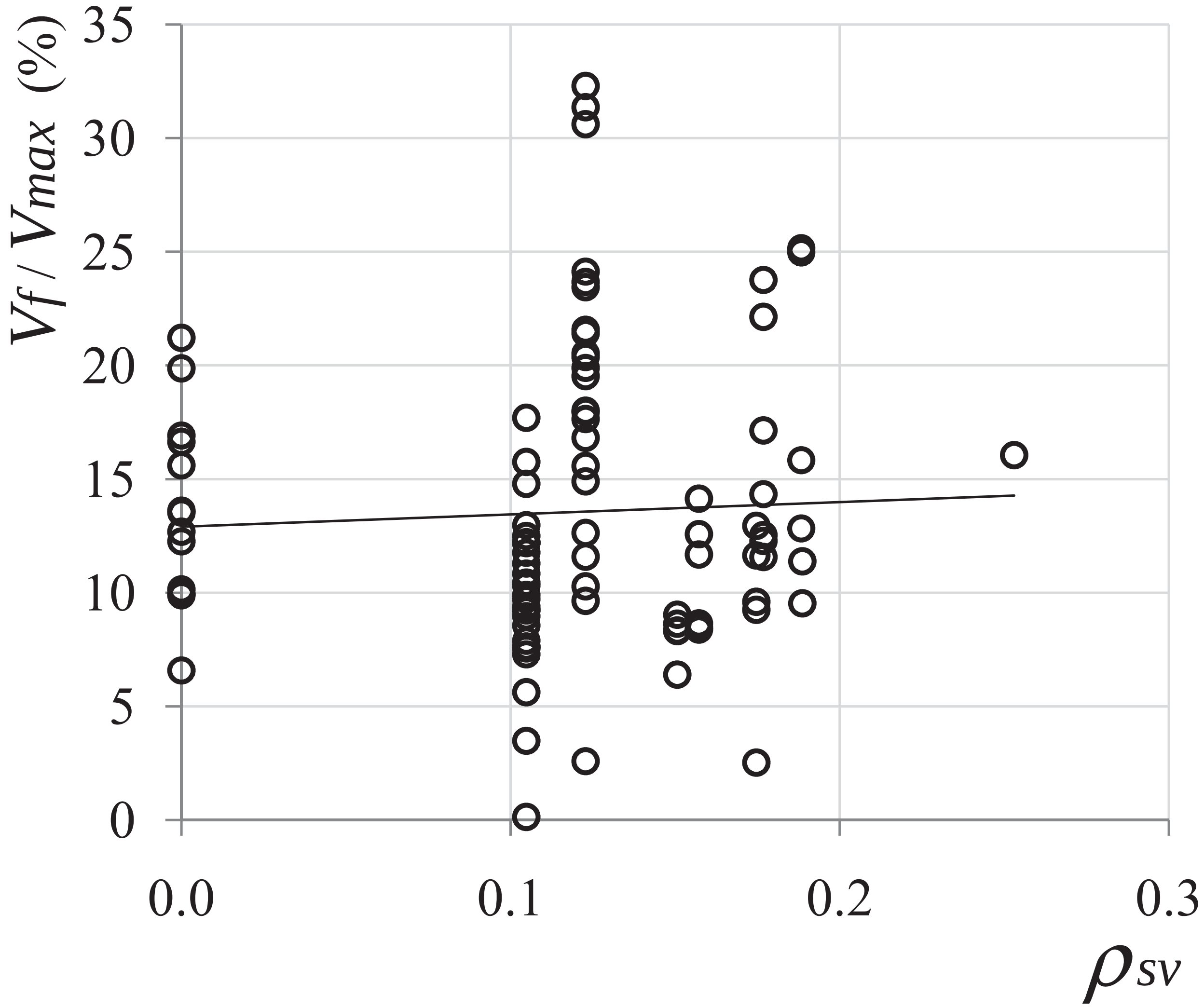

Figure 10
Click here to download Figure: Fig. 10.pdf

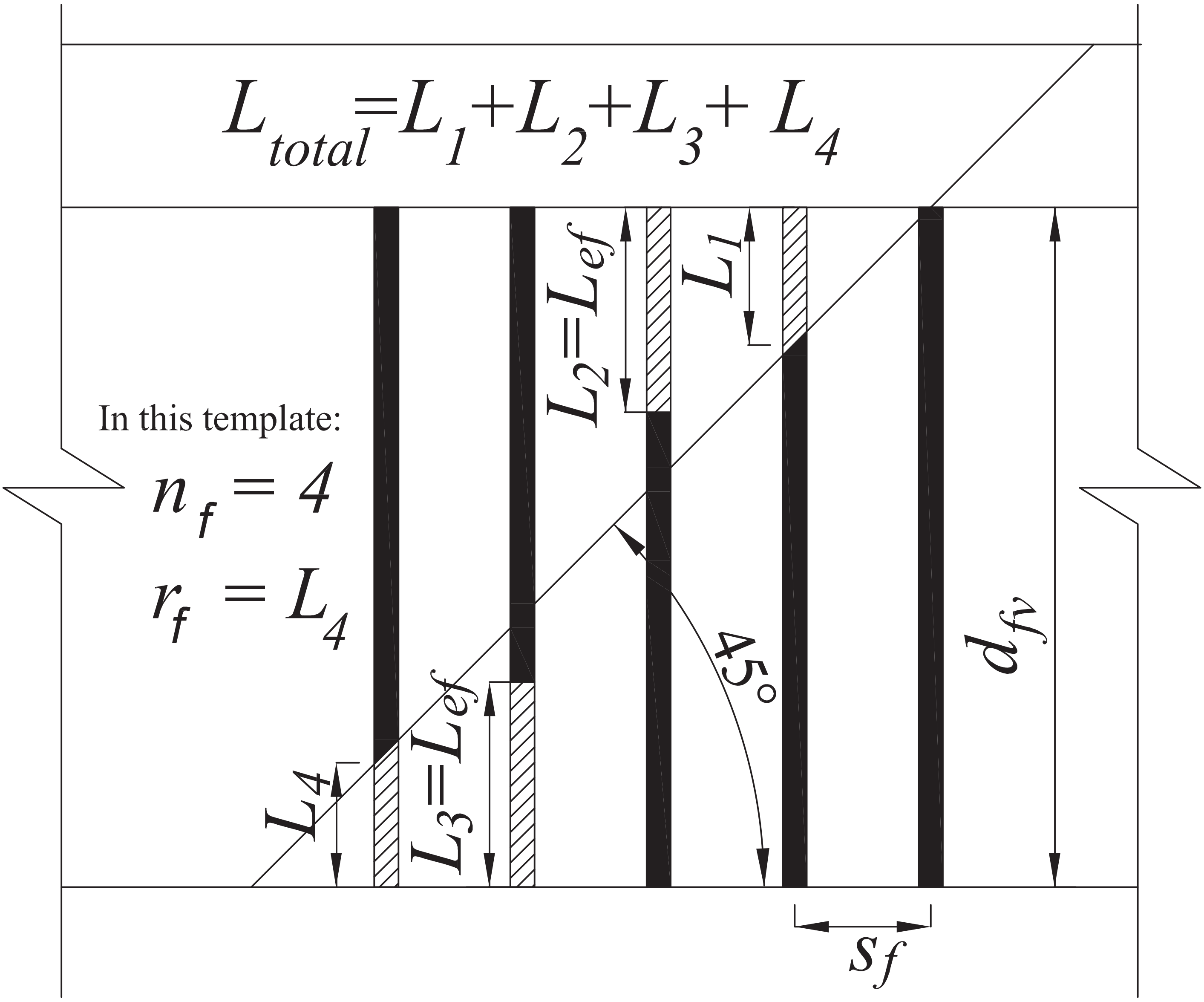

Figure 11a
Click here to download Figure: Fig. 11a.pdf

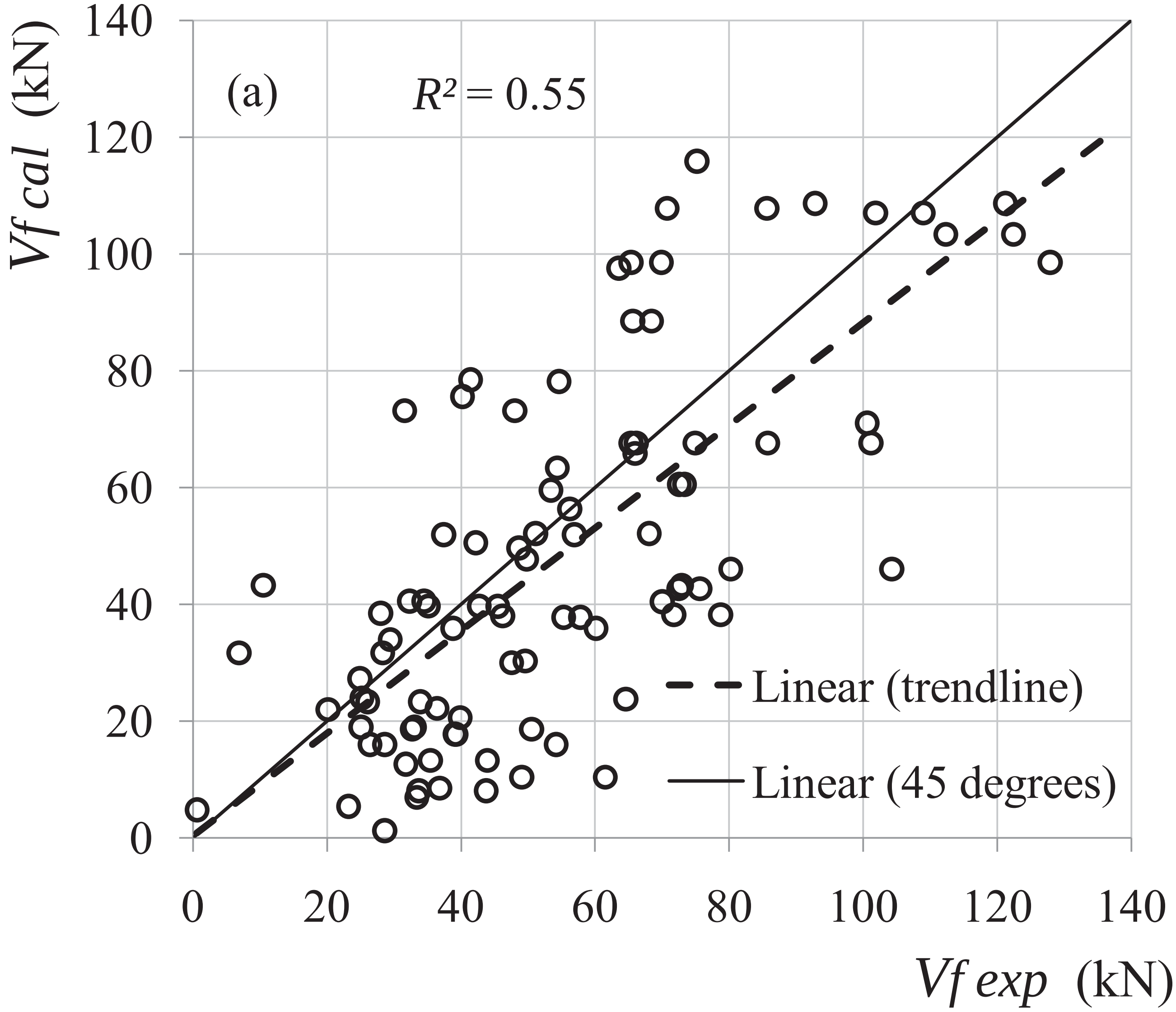

Figure 11b
Click here to download Figure: Fig. 11b.pdf

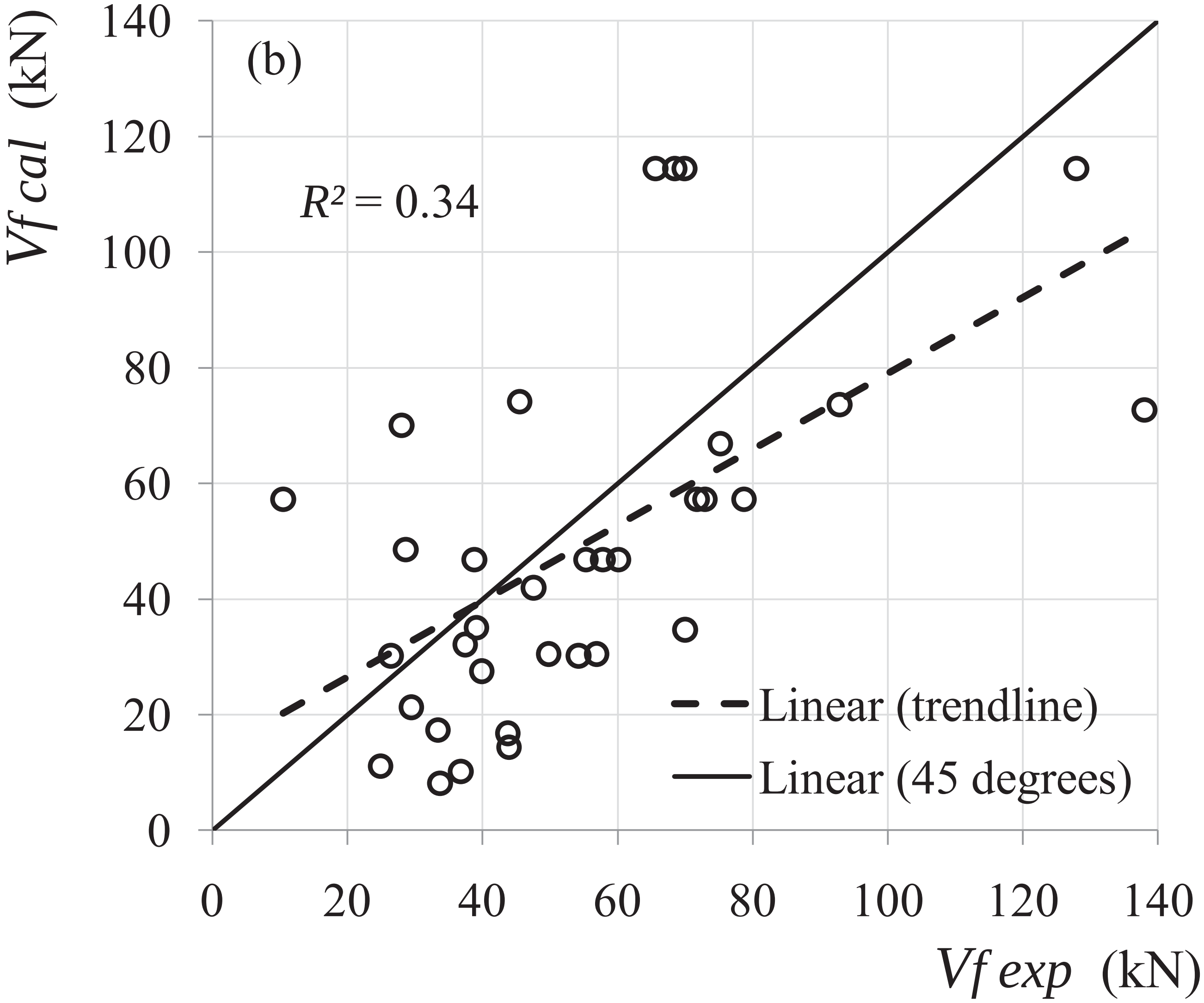

Figure 11c

Click here to download Figure: Fig. 11c.pdf

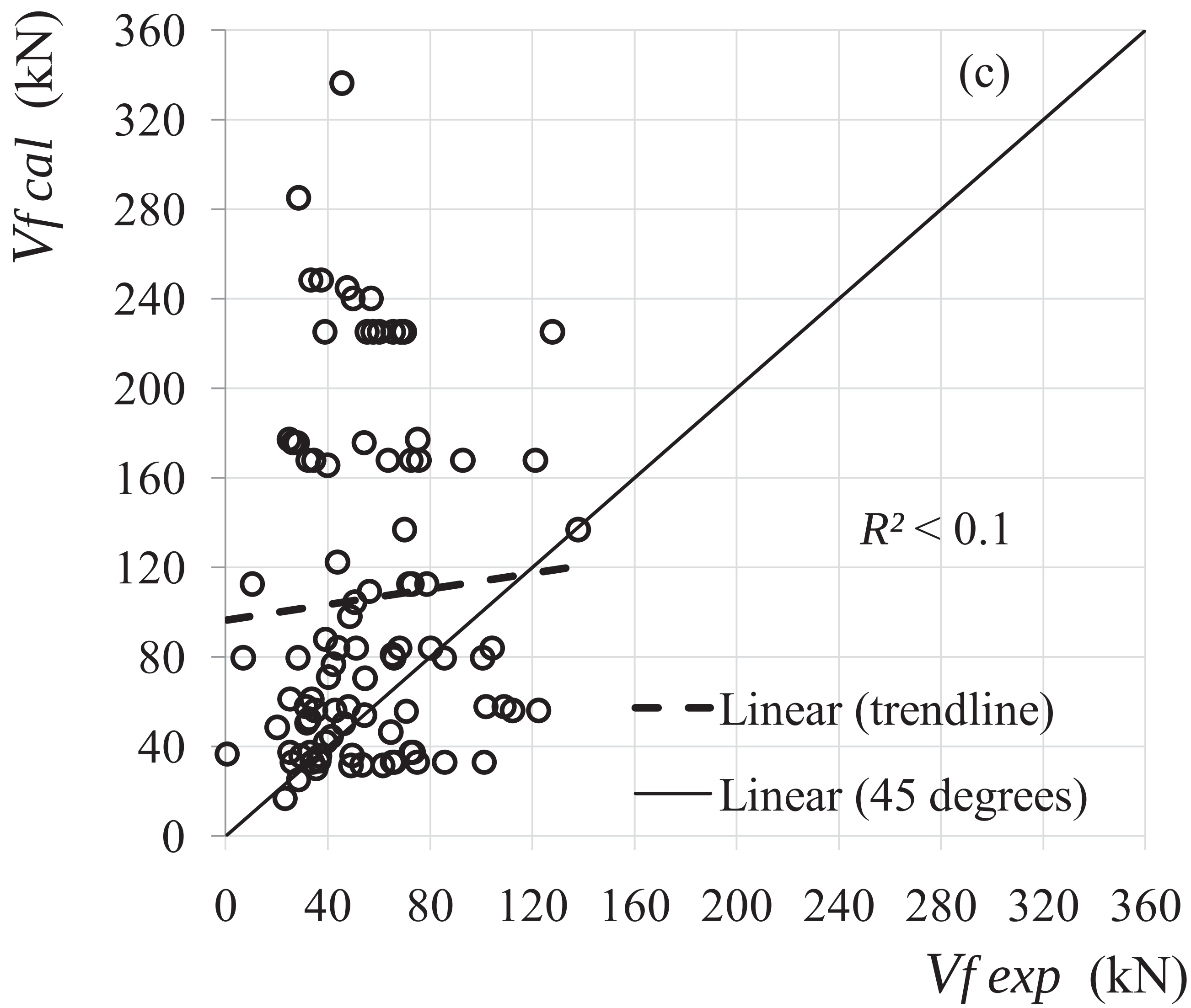

Figure 11d
Click here to download Figure: Fig. 11d.pdf

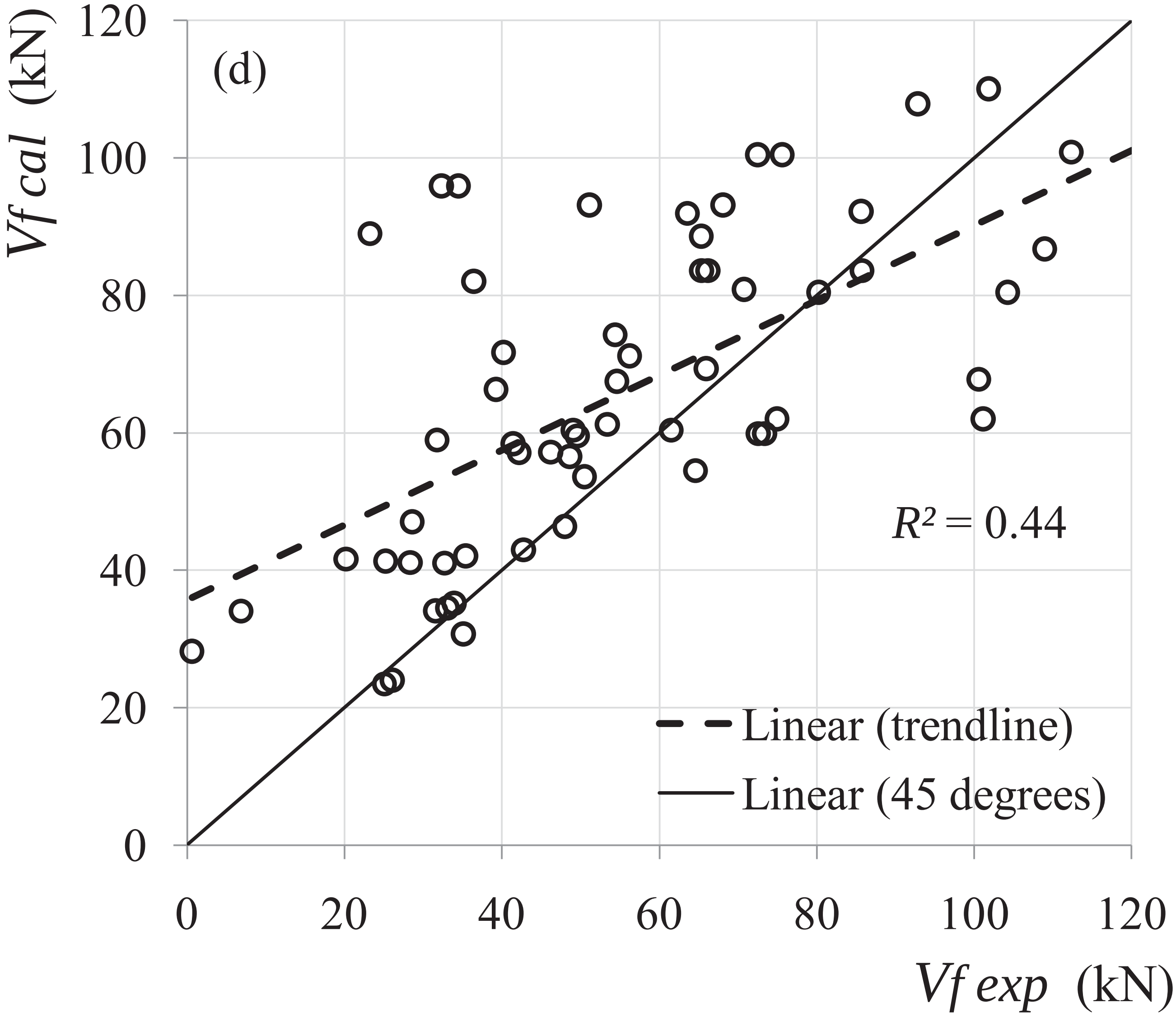

Figure 11e
Click here to download Figure: Fig. 11e.pdf

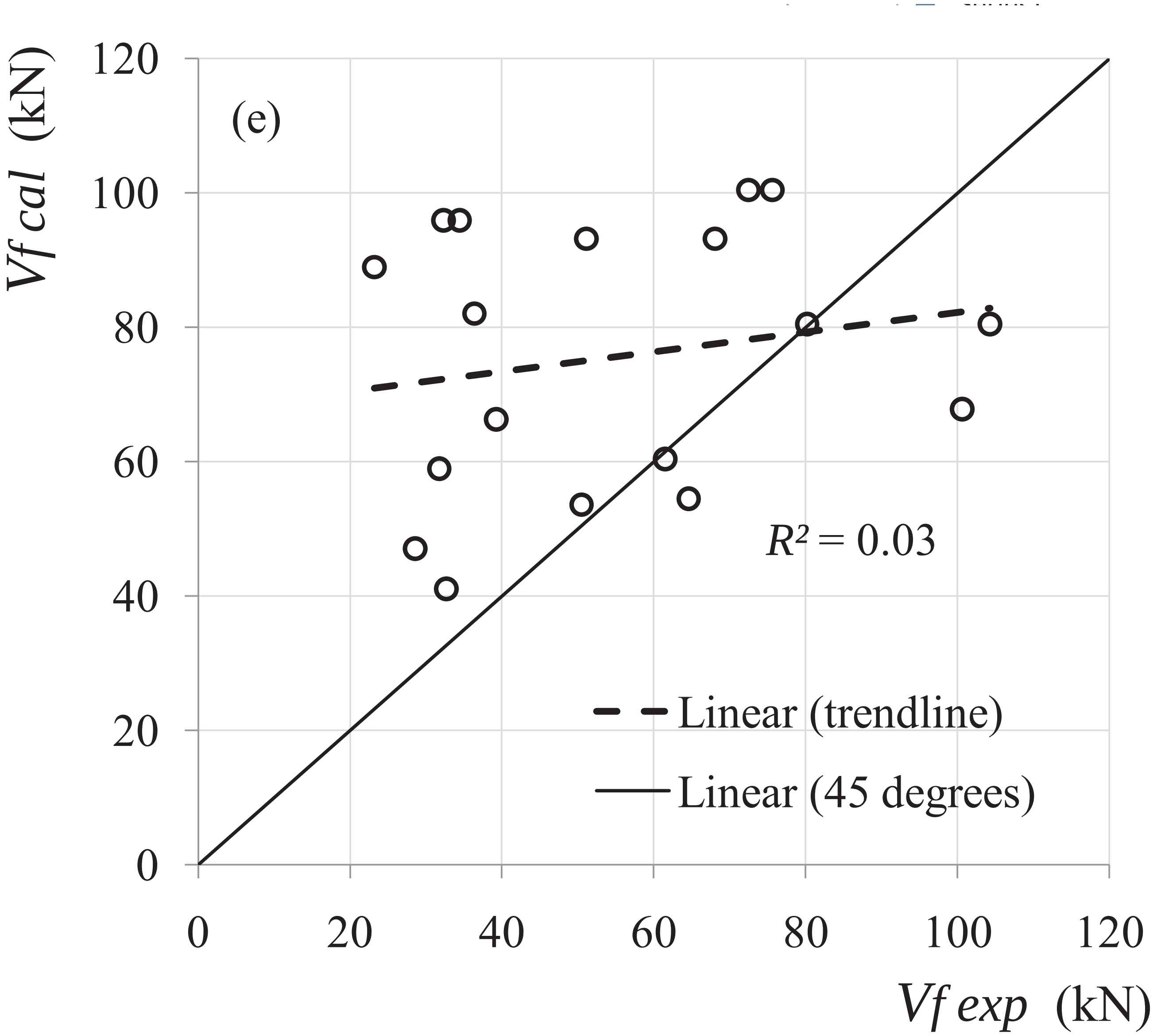

Fig. 1: Details of the tested specimens: (a) elevation; (b) cross-section of specimens with no steel stirrups; and (c) cross-section of specimens with steel stirrups. Dimensions in mm.

Fig. 2: Distributed diagonal cracking in specimen MR-NSM.

Fig. 3: Load versus maximum deflection at the load point.

Fig. 4: Load versus maximum strain in the steel stirrups: MR and HR series.

Fig. 5: Load versus maximum strain in NSM FRP rods in each side of the web for all the strengthened specimens.

Fig. 6: Distribution of ultimate strains in the stirrups within the failure zone

Fig. 7: Distribution of maximum strains in the CFRP rods.

Fig. 8: Contribution of FRP to the shear resistance versus steel stirrups reinforcement ratio (the straight line is the linear trend line).

Fig. 9: FRP strengthening factor $\kappa_f = V_f / V_{max}$ versus steel stirrups reinforcement ratio (the straight line is the linear trend line).

Fig. 10: Calculation of L_{total} for RC beams strengthened with NSM FRP.

Fig. 11: Predicted versus experimental result using (a) the proposed model; (b) De Lorenzis and Nanni (2001) for NSM FRP rods; (c) Anwarul Islam (2009); (d) Dias and Barros (2013) for laminates; and (e) Dias and Barros (2013) for laminates (the experimental results that are directly used to calibrate the model are not considered in comparison).